Final Technical Report

1 July 1970 - 30 June 1971

NEW METHODS FOR GROWTH AND CHARACTERIZATION OF

GaAs AND MIXED III-V SEMICONDUCTOR CRYSTALS

University of Southern California
Los Angeles, California 90007

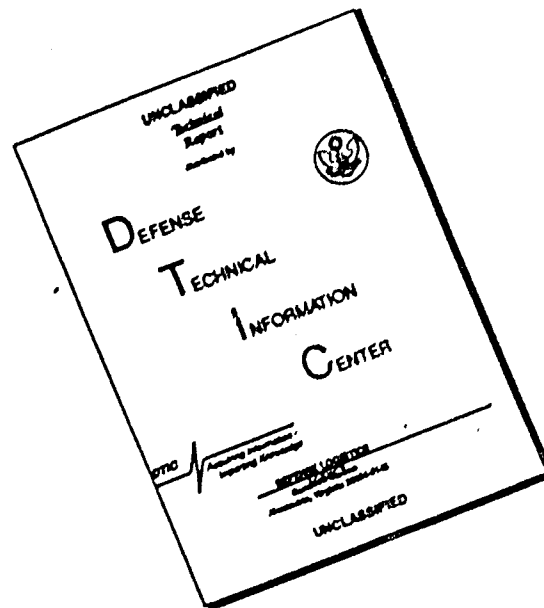Submitted to

ADVANCED RESEARCH PROJECTS AGENCY

ARPA Order Number 1628
Grant Number DAHC 15-70-G-14
1 July 1970 - 30 June 1971
$184,586.00

Principal Investigator: William R. Wilcox
                          (213) 746-6203

96

DISCLAIMER NOTICE

THIS DOCUMENT IS BEST QUALITY AVAILABLE. THE COPY FURNISHED TO DTIC CONTAINED A SIGNIFICANT NUMBER OF PAGES WHICH DO NOT REPRODUCE LEGIBLY.

DOCUMENT CONTROL DATA - R & D

(Security classification of title, body of abstract and indexing annotation must be entered when the overall report is classified)

1 ORIGINATING ACTIVITY (Corporate author)	2a. REPORT SECURITY CLASSIFICATION
Electronic Sciences Laboratory University of Southern California Los Angeles, California 90007	UNCLASSIFIED
	2b. GROUP

3 REPORT TITLE

NEW METHODS FOR GROWTH AND CHARACTERIZATION OF
GaAs AND MIXED III-V SEMICONDUCTOR CRYSTALS

4 DESCRIPTIVE NOTES (Type of report and inclusive dates)

Final Technical Report (1 July 1970 - 30 June 1971)

5 AUTHOR(S) (First name, middle initial, last name)

W. R. Wilcox

6 REPORT DATE	7a. TOTAL NO. OF PAGES	7b. NO. OF REFS
August 19, 1971	76	52

8a. CONTRACT OR GRANT NO	9a. ORIGINATOR'S REPORT NUMBER(S)
DAHC 15-70-G-14	
b. PROJECT NO ARPA Order No. 1628	
c.	9b. OTHER REPORT NO(S) (Any other numbers that may be assigned this report)
d.	

10 DISTRIBUTION STATEMENT

This document has been approved for public release
and sale; its distribution is unlimited.

11 SUPPLEMENTARY NOTES	12. SPONSORING MILITARY ACTIVITY
	The Advanced Research Projects Agency, Arlington, Virginia 22209

13 ABSTRACT

A new Czochralski technique for growing bulk gallium arsenide crystals has been invented and developed. A new technique for drying B_2O_3 for liquid encapsulation has been developed. It was discovered that surface moisture on vitreous B_2O_3 can be removed by exposing the material to a vacuum at room T. Improved smoothness of this films of GaAs grown by liquid epitaxial growth was achieved by adding arsenic to the hydrogen during growth. Alloy films have been grown and filed effect transistors have been produced.

Glow discharge spectroscopy was developed into an analytical technique for measuring and profiling the concentrations of constituents in this films. Theoretical advances have been made in the behavior of Schottky barriers. New polishing techniques, techniques for producing reliable ohmic contacts, and for orienting crystals have been developed.

DD FORM 1473
I NOV 65

14 KEY WORDS	LINK A		LINK B		LINK C	
	ROLE	WT	ROLE	WT	ROLE	WT
Gallium arsenide						
Semiconductors						
Crystal Growth						
Schottky barriers						
Impurity analyses						

NOTICE TO USERS

SUMMARY

The purpose of this program is to develop new and improved methods for the growth and characterization of gallium arsenide (GaAs) and mixed III-V semiconductor crystals.

A new Czochralski technique for growing bulk gallium arsenide crystals has been invented and is being developed. This should enable us to routinely produce III-V semiconductor crystals of higher quality than presently available. A new technique has been developed for drying encapsulation materials, such as B_2O_3, for use in III-V crystal growth. More rapid and convenient drying is obtained than with previous techniques. It has been discovered that surface moisture on vitreous B_2O_3 can be removed by merely exposing the material to a vacuum at room temperature. The evaporation rate of a melt was found to vary with the inverse one-third power of the total pressure, which corresponds to turbulent free convection.

Improved smoothness of thin films deposited by liquid epitaxial growth was achieved by adding arsenic to the hydrogen atmosphere during growth. $GaAs_{1-x}Sb_x$ and $Ga_{1-x}In_xAs$ alloy films have been grown with x up to 0.13 for In and up to 0.18 for Sb. Vegard's law was found to be valid for $GaAs_{1-x}Sb_x$. Photoluminescence data for these alloys indicated impurity-band transitions. Photoluminescent efficiencies were encouragingly good, i.e., within a factor of 10 of solution-grown GaAs. Gallium arsenide field effect transistors were produced by our liquid epitaxial growth techniques. Low reverse-biased leakage currents were obtained and found to be associated with a highly regular substrate-film interface.

Films of a related compound, GaN, have been grown by chemical vapor deposition on sapphire substrates. Carrier concentrations are too high - about $10^{20}/cm^3$ - for unknown reasons. Highly efficient photoluminescence has been observed in these films both at low temperatures and at room temperature.

Glow discharge spectroscopy was developed into an analytical technique for measuring and profiling the concentrations of constituents in thin films. For Sn in GaAs, for example, the detection limit is 3×10^{16} atoms cm^{-3} or 0.4 ppm by weight. Sputtering yields varied with orientation in the following order: (111)As, (111)Ga, (211), and (110). In addition, we have shown that emission spectroscopy is a quick and sensitive method for measuring sputtering rate.

An improved method has been developed for interpreting data on photo-emission from Schottky barriers. Such results aid in analysis of impurity and interface effects as well as for measuring the barrier height of semiconductors. Theoretical and experimental methods are under development for determining the presence and behavior of deep-lying impurities by use of capacitance-voltage-frequency measurements.

Our GaAs crystals are also being studied by dislocation etch pits, X-ray topography, electron microprobe methods and Hall-effect measurements.

An improved polishing technique has been developed using sodium hypochlorite on a special polishing pad. When used in a special lapping apparatus, substrate thicknesses down to 10 micrometers can be obtained. We have developed a technique for producing reliable metal contacts on GaAs. Plating from a molten salt bath is utilized. A new and simpler method has been developed for orienting III-V crystals. Reflection of a laser beam from cleavage surfaces is utilized.

The following pieces of capital equipment have been purchased under this grant and are now in operation: Cryogenic temperature controller, dewar and accessories, digital voltmeter, high purity water system, balance, vacuum pumps (2), vacuum oven, zone refiner, X-ray topographic camera, high voltage power supply, temperature controllers (3).

RESPONSIBLE STAFF

Staff	Responsibility	Sections in Report
W. R. Wilcox	Program coordination, research in crystal growth.	I - C, D, G
W. P. Allred	Growth of bulk crystals.	I - A, B
J. M. Whelan	Liquid epitaxial growth and characterization.	I - E, I, J II - B
M. Gershenzon	Photoluminescence, GaN growth.	I - F II - H
H. Stover*	Device fabrication.	I - H, J
R. Wang	Observation of dislocations and study of influence on electronic properties.	II - A
D. B. Wittry	Electron microprobe studies.	II - C
C. R. Crowell	Electronic properties.	II - D, E, F, G

*No longer at USC.

CONTENTS

I. MATERIALS PREPARATION

A. New Czochralski Technique

The primary problem in pulling bulk crystals of gallium arsenide is avoidance of arsenic evaporation from the melt. In the past this has been accomplished by two techniques. In the oldest technique the crucible, crystal, and pull rod were located inside a quartz chamber held at a sufficiently high temperature that condensation of arsenic did not occur on the walls. The pull rod was coupled magnetically to an external drive system which allowed both rotation and vertical motion. Irregular rotation and pulling resulted. To avoid this, the liquid-encapsulated Czochralski technique was developed several years ago. A layer of molten B_2O_3 was placed on the surface of the GaAs melt to prevent evaporation. Crystals were pulled through the B_2O_3. Unfortunately, the B_2O_3 layer blurred the view of the melt-crystal miniscus making control difficult. Molten B_2O_3 also adhered to the crystal and later generated stresses due to differences in thermal expansion.

We have invented and built a Czochralski apparatus which overcomes these difficulties.[*] The new grower, shown schematically in Figure 1, uses a direct drive similar to that used in conventional Ge and Si growers. The smoothness of rotation and pull is limited only by the mechanical system. The pull rod rotates through a B_2O_3 or other liquid seal in a close-fitted tube. The molten glass is necessary to prevent the loss of arsenic from the pulling chamber during growth. It is the use of the push-pull rotating seal (which can operate at 600°C and above) which allows the magnetic puller to be replaced. Since the B_2O_3 is not in contact with the GaAs, as in liquid encapsulated growth, it is not necessary to start with pre-reacted GaAs. Gallium and arsenic in stoichiometric amounts are simply inserted into the crucible and reacted in situ. The construction of the new system involves only simple glass-blowing, with no precision quartz or glass-blowing required.

In the early experiments, arsenic tended to leak through the B_2O_3 seal. This was caused by water which was present in the B_2O_3. The water reacted with the arsenic vapor to form an oxide which dissolved in the B_2O_3 and was readily transported through the seal to the vacuum chamber above. The problem was solved by heating the B_2O_3 in a vacuum within the system, thus preventing

---

[*] U.S. Patent applied for. We recently learned that workers at the Royal Radar Establishment in England have invented a similar apparatus, for which a U.K. patent has been applied .
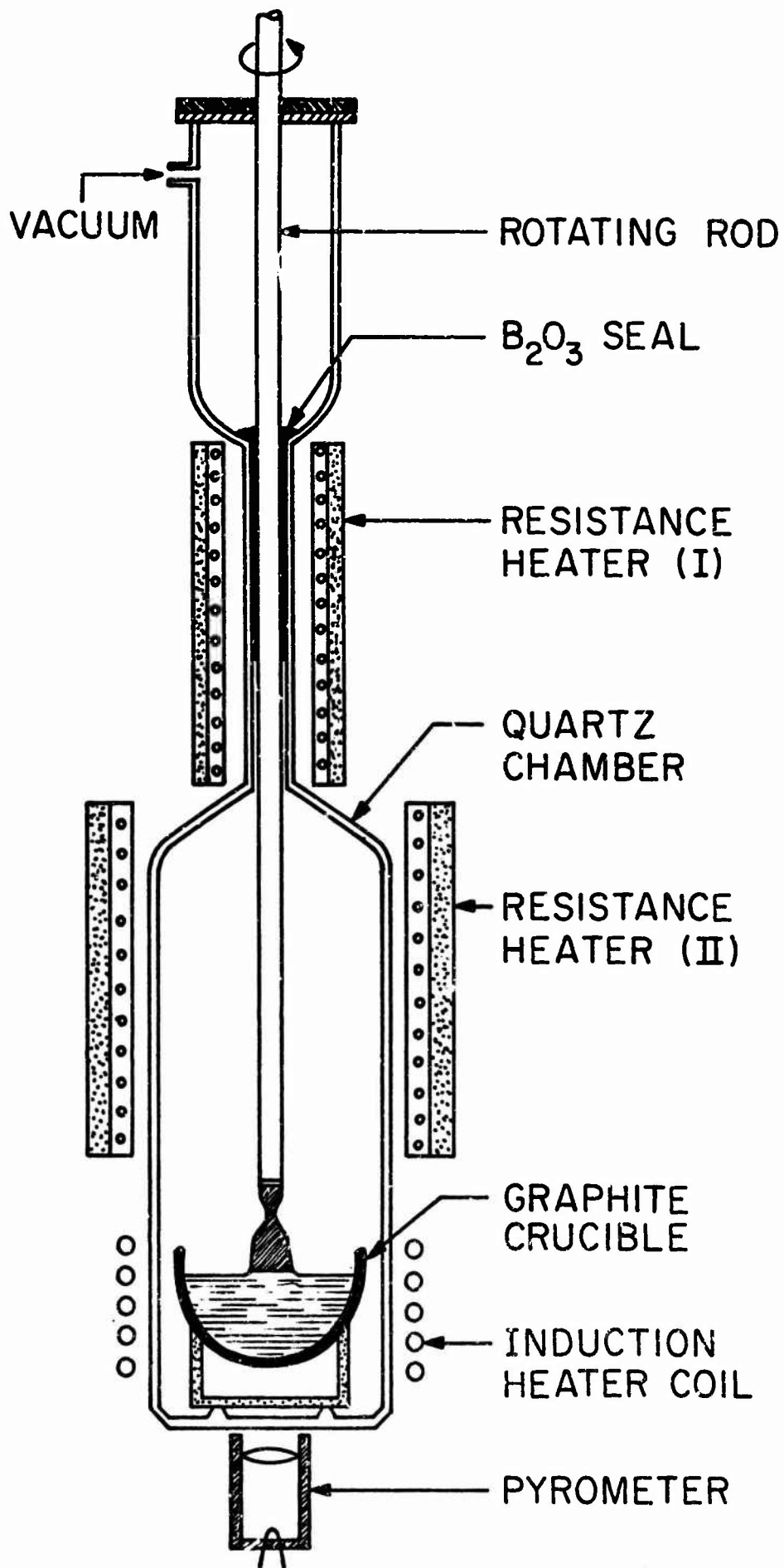
VACUUM

ROTATING ROD

B_2O_3 SEAL

RESISTANCE HEATER (I)

QUARTZ CHAMBER

RESISTANCE HEATER (II)

GRAPHITE CRUCIBLE

INDUCTION HEATER COIL

PYROMETER

Fig. 1   New Czochralski Apparatus

2

pick-up of H_2O during the loading process. The B_2O_3 was further purified by first bleeding dry helium into the pulling chamber before melting of the B_2O_3 and then passing the helium up through the molten B_2O_3 at 900°C. This process was very effective in removing residual water from the B_2O_3. Arsenic leakage was also caused by channeling of the B_2O_3. The channels were formed when the pull rod was pushed down into the pulling chamber. The B_2O_3 tended to run down one side of the pull rod, leaving a void on the other side and permitting loss of arsenic. The channeling was eliminated by using helium pressure to push the B_2O_3 down around the pull rod in an even manner. Arsenic loss through the B_2O_3 seal is no longer a problem.

A problem of poor visibility due to evaporated deposits was corrected by the addition of an eye port which is heated to about 900°C by a resistance heater. The window of the eye port now remains clear during the entire growth period.

Crystals of GaAs are now being grown weekly. Resistivity measurements on undoped crystals showed a resistivity of 10^8 ohm cm. The Hall coefficient of these samples were not obtained due to the high resistivity of the material.

A major limitation of the purity of the material is that of contamination from the crucible. A spectrographic analysis of a vitreous carbon crucible along with an analysis of a gallium arsenide crystal grown in similar material is shown in Table 1.

TABLE 1. SPECTROGRAPHIC ANALYSIS OF A VITREOUS CARBON
CRUCIBLE AND OF A GALLIUM ARSENIDE CRYSTAL
GROWN IN A SIMILAR CRUCIBLE*

Element	Crucible (ppm)	Gallium Arsenide (ppm)
Fe	ND (< 50)	260
Cu	1.5	ND
Al	29	ND
Ca	66	TR (< 2)
K	TR (< 1500)	ND
Si	TR (< 10)	180
Mg	8.4	ND

*ND = Not Detected
TR = Trace

From a comparison of the analysis there appears to be considerably more contamination of the gallium arsenide with Cu, Al, Ca, K and Mg than could arise from the crucible. The source of this contamination has not yet been determined. There are several possible explanations that might be offered. (1) The boat material is nonuniform; thus any one analysis would not be representative of the purity of the material. (2) The B_2O_3 used as an arsenic seal is a source of contamination, or (3) the quartz system is contributing to the source of the contamination. These possibilities are being investigated.

Dislocation densities of crystals grown in this new system have been measured by etch pit and topographic techniques (see Section IIA). Dislocation densities are low, with the latest crystal averaging < $100/cm^2$ and with sizeable volumes dislocation-free.

B. Liquid-Encapsulated Floating-Zone Melting

In all of the Czochralski techniques just described, the melt is contained in a crucible and so is contaminated somewhat by the crucible material. Silicon also appears to be transported from the quartz container. We propose to avoid these difficulties by development of liquid-encapsulated floating-zone melting. The apparatus design is shown in Figure 2. The melt will contact only B_2O_3 or another encapsulant, which will not only prevent evaporation but should also act as a getter for impurities. We therefore expect to be able to produce bulk GaAs of higher purity and higher mobilities than produced previously. An encapsulant with a density near that of molten GaAs would permit zone melting of large ingots.

Construction of this apparatus is nearly complete. We will test it first on GaAs with B_2O_3 as an encapsulant. Other encapsulants of higher density will then be sought. Mixed III-V material will eventually be attempted.

C. Drying of Encapsulants

As noted above, it is important to remove traces of moisture from the encapsulant to avoid reaction with the semiconductor melt and vapors. Previous techniques for drying B_2O_3 utilized long exposure to high vacuums at elevated temperature. The initial heating produced troublesome frothing. Addition of reactive metals was sometimes employed to hasten drying. We have developed two drying techniques that are rapid and require no addition of reactive metals.
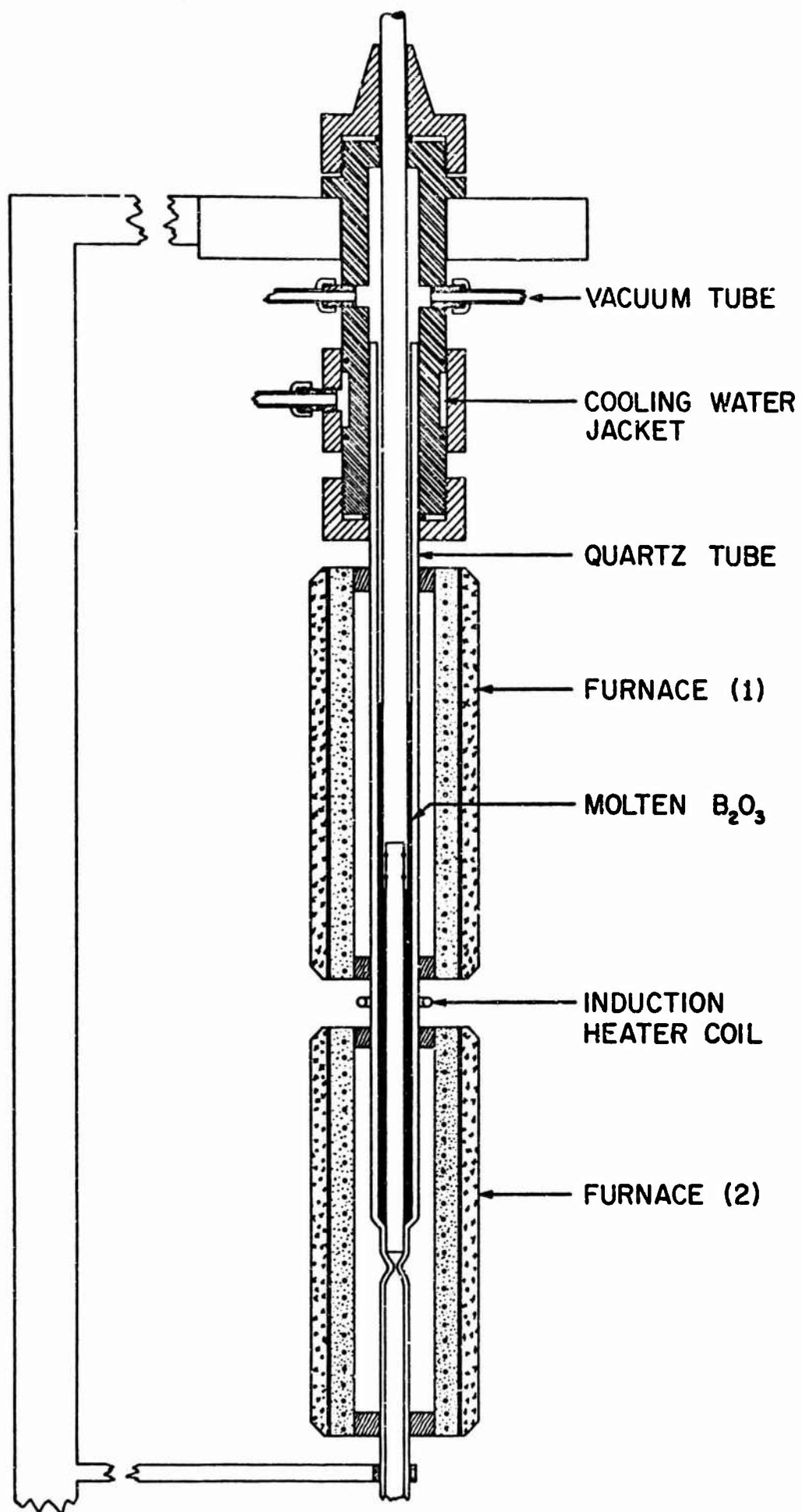
VACUUM TUBE

COOLING WATER JACKET

QUARTZ TUBE

FURNACE (1)

MOLTEN B₂O₃

INDUCTION HEATER COIL

FURNACE (2)

4-A

Figure 2. Preliminary Design of Liquid-Encapsulated Floating-Zone Melting

Apparatus

As-received boric anhydride reagent was found to contain approximately 3 wt % moisture. In one drying technique, boric anhydride powder was charged into a carbon crucible to about two-thirds full, and slowly heated in dry nitrogen gas at one atmosphere pressure. When the frothing began, at a temperature of 700 to 800°C, the bubbles were broken with a rod. When the formation of bubbles subsided sufficiently, the temperature was again slowly raised up to 1200°C. During this period, bubbling of dry N_2 gas through the B_2O_3 melt was started. Dry gas was not effective below 1000°C because the gas flowed through a channel formed in B_2O_3 due to the high viscosity of the melt. Around a temperature of 1200°C, good bubbles formed and agitated the melt very vigorously. The dry gas bubbles not only entrained the water-vapor bubbles produced in the melt, but also accelerated the rate of mass transfer by continuous renewal of the dry gas-B_2O_3 interface. After completion of drying, the melt was cooled very slowly to avoid trapping of suspended gas bubbles in solid B_2O_3.

Chemical reaction between the carbon of the crucible wall and H_2O in B_2O_3 is expected above 1000°C. For example, Poch[1] dried B_2O_3 in a vacuum by the following consecutive steps.

(i) Twelve hours in a platinum crucible (shallow) at 850°C and 1 atmosphere.

(ii) Five hours in a platinum crucible at 1300°C and 1 Torr.

(iii) Six hours in carbon crucible at 1300°C/1 Torr.

The minimum H_2O content attained by the above method was 10 ppm by weight, which is the lowest value found in the literature.

A recent improvement to our drying technique was to predry the powdered B_2O_3 in a vacuum oven before melting it. About 200 g of B_2O_3 was charged into a carbon crucible and treated in the vacuum oven for 3 days. The temperature was gradually raised from 150 to 225°C in order to avoid sintering of B_2O_3 powder.[2] This treatment removed about 50% of the water. More significantly, this material did not froth when melted!

Some advantages of using predried powder in the N_2 bubbling process of drying B_2O_3 are:

1. The mechanism to break bubbles is not required.

2. The amount of B_2O_3 to be dried can be increased as desired for one-batch operation.

3. The loss of B_2O_3 via volatile forms of boric acid[3] during the frothing period is significantly reduced.

Trace water in fused B_2O_3 was measured by infrared transmission measurements. In order to produce suitable samples, sheets of B_2O_3 glass were slowly pulled in air from the melt both preceding and following drying. In an attempt to calibrate the infrared absorption, some of the sheets were exposed moist air. The amount of moisture introduced was estimated by weighing samples. Typical infrared transmission curves are shown in Figure 3. It may be seen that water was responsible for two different bands in B_2O_3, one at 2.84 μ and one at 3.13 μ. The 3.13 μ absorption was increased by exposure of samples to moist air while the 2.84 μ band was not significantly altered. Exposure to a vacuum at room temperature caused the 3.13 μ transmission to slowly increase until it was the same as before exposure to humid air. The 2.84 μ band was unaffected by vacuum. Thus it was concluded that bulk moisture was responsible for absorption at 2.84 μ while surface moisture was responsible for infrared absorption at 3.13 μ. Indeed, a thin surface deposit was observed and is thought to be boric acid.

These results may be compared with previous infrared absorption measurements using B_2O_3 with large amounts of water present internally.[4] Using an extinction coefficient of 141 1/mole cm., a bulk moisture concentration of 610 ppm is calculated for the sample of Curve 1 in Figure 3. From the fact that the solubility of water in molten B_2O_3 is proportional to the square root of the vapor pressure,[4] we estimate an equilibrium water content of 780 ppm at 730°C, 65% relative humidity (at room temperature).

We are now measuring the rate of water absorption in fused B_2O_3 in air and the rate of water removal in vacuum at room temperature.

D. Travelling-Heater Method

In the travelling-heater method (THM), a solvent zone is slowly moved through solid feed material by movement of a heater, as in Figure 4. Because
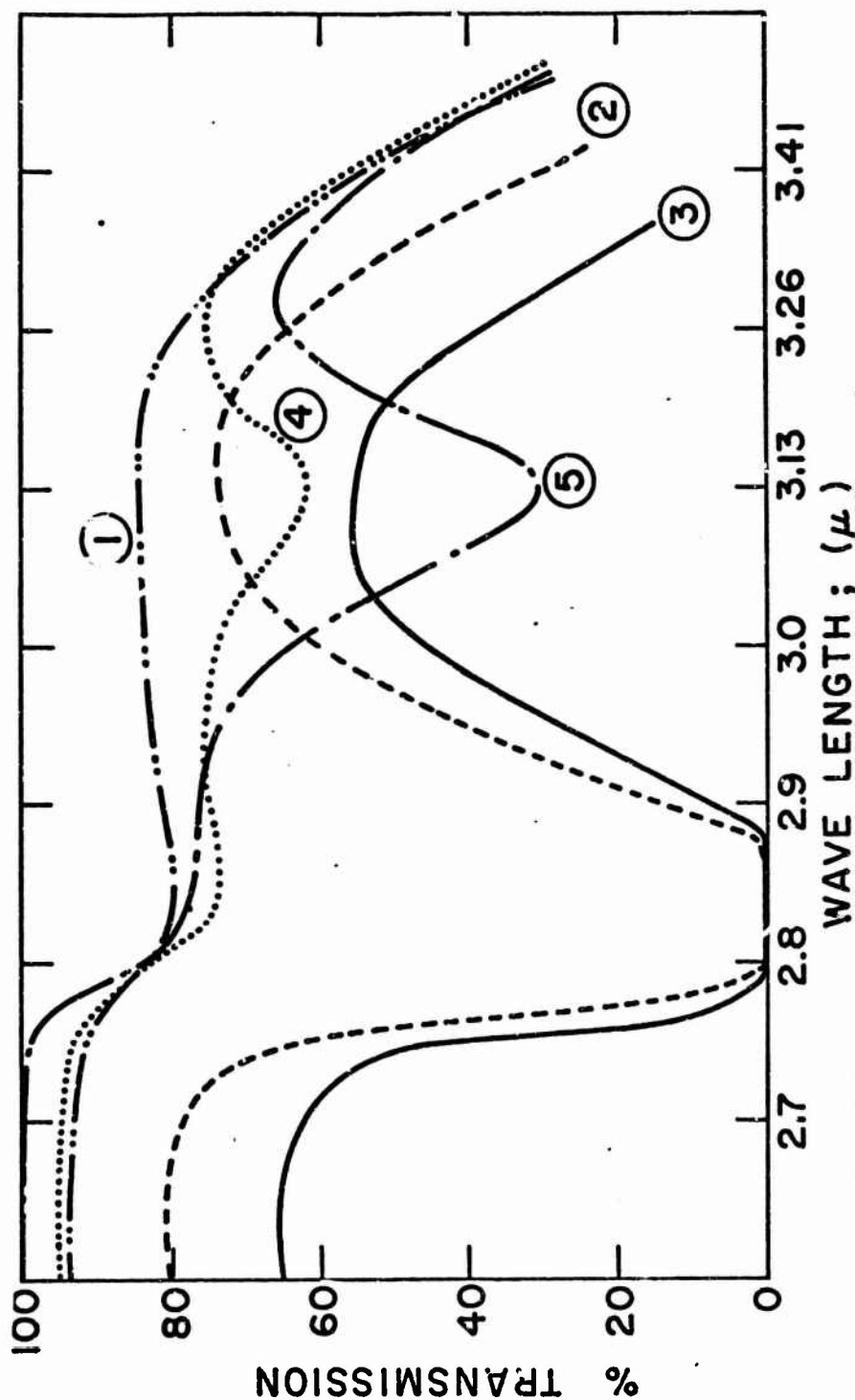
Figure 3. Infrared Transmission curves for vitreous boron oxide samples

Curve 1: Dried by bubbling dry N_2 at 1200°C for 10 hours. 0.114 mm thick

Curve 2: Heated at 900°C for 1 hour. 0.259 mm thick
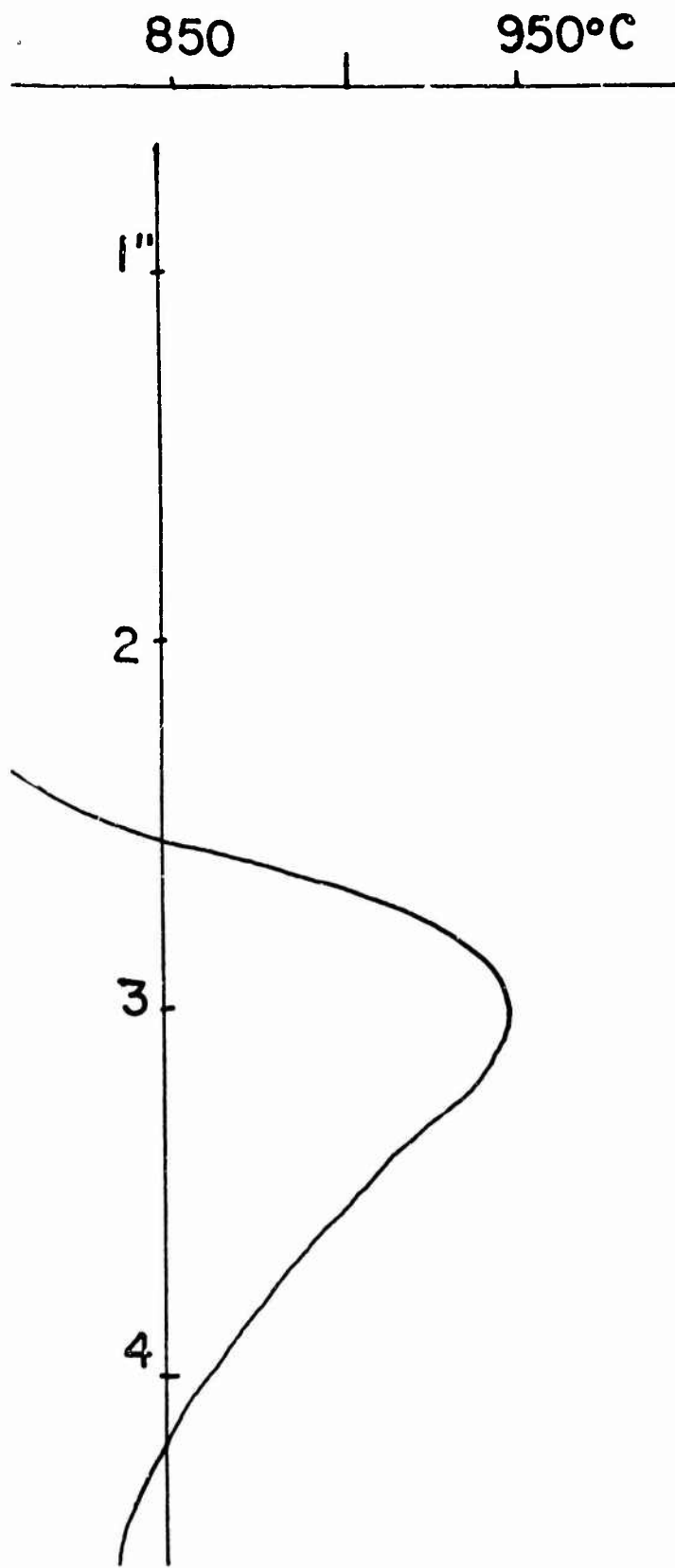
Curve 3: Dry N_2 bubbled through for 1 hour at 950°C. 0.528 mm thick

Curve 4: Dried sample with 0.011 wt. % surface moisture. 0.104 mm thick

Curve 5: Dried sample with 0.038 wt. % surface moisture. 0.116 mm thick

6-A

850   950°C

1"

2

3

4

Temperature profile in empty

heating chamber.

GaAs
FEED

RESISTANCE
HEATER

Ga MELT

GaAs
SEED

Figure 4. Travelling Heater Method Apparatus.

6-B

of the solvent, the temperatures are much lower than when melt growth techniques are utilized. This greatly lessens problems with attack of the container, with vaporization of volatile components, and with thermal strain and resultant defect formation. The zone leveling configuration also makes possible growth of mixed III-V crystals without the composition gradients produced in the normal freezing methods (e.g., Czochralski and Bridgman techniques).

Previous work, primarily at Tyco Laboratories, has demonstrated the feasibility of THM for growth of compounds and mixed crystals. Very little has been published on the phenomena governing THM crystal growth or on the properties of the materials produced thereby. We intend to fill these gaps in crystal growth knowledge, and thereby to enable growth of better crystals. At the present time we feel that we have come abreast of the current state of the art on THM growth.[5] Single crystals of GaAs can routinely be produced both with and without seeding, although polycrystalline ingots are occasionally obtained. Figure 5 shows that crystal perfection is improved by THM growth. Our polycrystalline ingots are not homogeneous, as shown by the electron microprobe scans of Figure 6.

In addition to growth of GaAs and mixed III-V's, future work will include studies of the heat and mass transfer aspects of THM growth. We feel, for example, that the shape of the crystallizing interface is the determining factor in whether the resulting ingot is single or polycrystalline. To test this, and to enable production of interface shape, low-temperature transparent organic analogs of THM are being studies (Figure 7) in conjunction with computer calculations of heat and mass transfer. We also plan to try THM by liquid-encapsulated floating-zone melting eventually.

E. Liquid Epitaxial Growth

The liquid epitaxial growth technique for producing thin films represents the only crystal growth method that was under investigation at USC before initiation of the present grant. Films are grown on GaAs substrates by slow cooling of Ga solutions in an isothermal environment. During this year, the surface texture and substrate-interface regularity of GaAs films were significantly improved by the addition of arsenic to the hydrogen atmosphere under which the solution growth occurs. This permitted the growth of smooth films on substrates with the desired orientations, (211) and (311), and moderate dislocation densities ($\sim 5000/cm^2$). Comparable results were previously obtainable
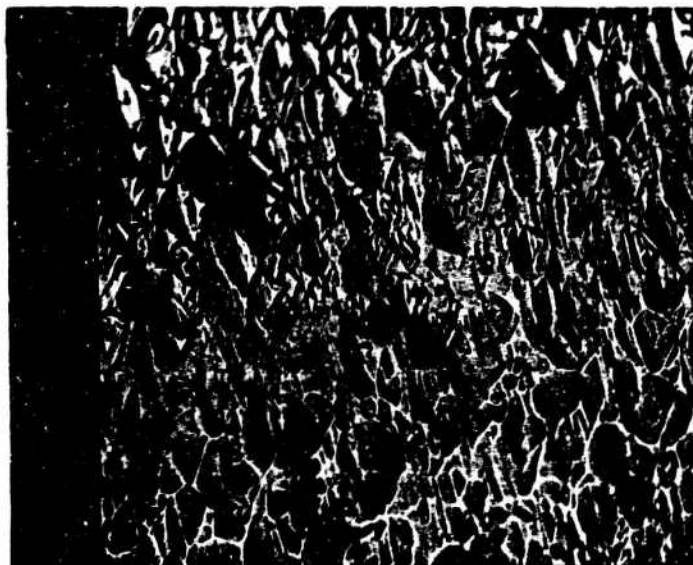
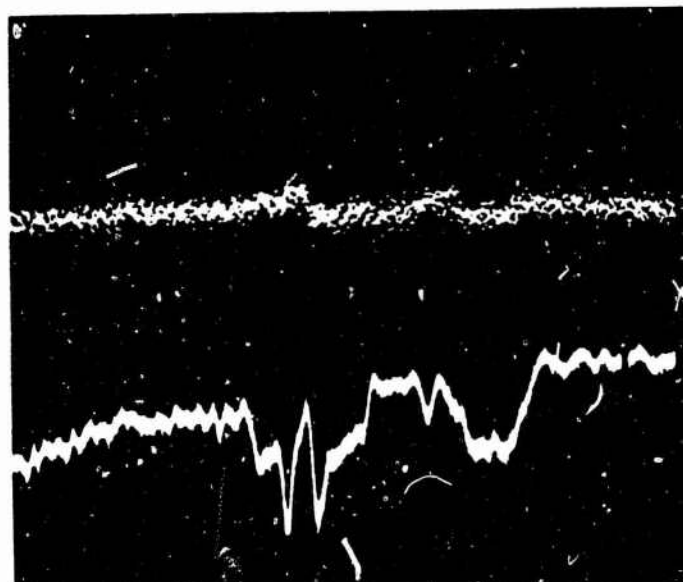A.   Melt grown seed

B.   THM grown crystal

Figure 5. Ga (111) etch pits

7-A

← LINEAR SCAN

A. Cathodoluminescence

NOT REPRODUCIBLE

← Te XRAY SPECTRUM

← BRIGHTNESS

B. Scans of tellurium X-ray spectrum and cathodoluminescence

brightness

Figure 6. Electron microprobe results on THM GaAs

7- B

Figure 7. Low-temperature transparent organic analog of THM.

with substrates with dislocation densities $\sim 100/cm^2$. (Smoothness is one factor which will ultimately limit the types of devices that can be fabricated from GaAs.)

Variables affecting the characteristics of thin alloy films on GaAs substrates were elucidated. These included the determination of the Ga-In-As liquidus-solidus curve at 860°C, evaluation of film quality as a function of the substrate orientation and a comparison in the nucleation characteristics of two alloy systems. GaAs substrates with (111) orientations were superior to all other orientations tried - (100), (110), (211) and (311). The density of nucleation centers was markedly greater for the $GaAs_{1-x}Sb_x$ alloys than for the $Ga_{1-x}In_xAs$ ones. For this reason the $GaAs_{1-x}Sb_x$ alloys are more likely to be useful when films ~ 1 µm thick are required with energy gaps more than 0.04 eV less than GaAs. Difficulty with undercutting dissolution of the substrate was encountered in growth of concentrated alloy films. Bulk alloy substrates are needed to avoid nucleation and undercutting problems, but are not yet available.

The dependence of lattice constant on compositions of $GaAs_{1-x}Sb_x$ alloys has been measured. A linear variation with x was found, corresponding to Vegard's Law. Previous data had indicated a strong deviation from a linear variation. The new results are attributed to the improved homogeneity of our solution-grown alloy films.

One remaining difficulty is the reduction of oxides on the substrate surface prior to growth. An apparatus is being constructed for doing this by using a biased zirconia tube as a crucible-oxygen pump. Reduction of oxygen levels in the growth system should permit growth at lower temperatures, which in turn would reduce the contamination problem and simplify thickness control.

The above improvements in thin film growth have been used to grow n-type layers on p-type GaAs substrates. The quality of the resulting pn junctions was excellent, as judged by low reverse biased leakage currents. Good junctions were associated with highly regular substrate-film interfacial surfaces. Growth conditions which compromised the resularity always resulted in pn junctions with enhanced leakage currents. Mesa GaAs junction field-effect transistors with a ring-dot configuration were built to demonstrate the gate junction quality of GaAs transistors with relatively large transconductances (6×10^{-3} mhos). The reverse currents at the pinchoff voltages (~ 12 V) were about 2×10^{-9} amp.

Maximum processing temperatures required on the epitaxial films were under 430°C. This is partly due to the satisfactory performance of the Au-Sn alloy contacts described in Section I-J.

F. Crystal Growth of Related Compounds[*]

Gallium nitride is a III-V semiconductor of current interest as a luminescent material. Several methods have been used to grow GaN single crystals. The most successful method has been an open-tube vapor phase growth technique, in which Ga, transported to the deposition zone as a gaseous halide, reacts with NH_3 to form GaN epitaxially on a sapphire substrate. The GaN layer thickness is about 50 μ. It is colorless and always n-type with carrier concentrations on the order of 10^{20} cm^{-3}. Recently our efforts have concentrated on the purification and the compensation of the crystals. First, oxygen was considered as the possible impurity. As GaN deposits attack quartz walls, the system is liable to become contaminated with Si and oxygen. Therefore, an alumina liner was put in the high-temperature reaction region and in the low-temperature deposition region. The ammonia was purified by passing it over a heated Na metal trap about 12 inches in length. The hydrogen tank was replaced with a hydrogen generator with purity of 10 ppb. However, with all those changes, no decrease was noted in the carrier concentrations. Later, water vapor was added intentionally to the growth system. It caused nucleation problems and produced yellow-colored crystals. All measurements indicated that there was no noticeable resistivity change.

Native defects such as nitrogen vacancies are now suspected to be the cause of the high carrier concentrations. This is because the GaN crystal growth depends so strongly on the substrate surface which catalytically dissociates the ammonia to generate the active nitrogen required for the reaction for crystal growth. We found that more than 98% of the ammonia passed through the growth system without reacting or dissociating into nitrogen and hydrogen.

We also added PH_3 during growth, hoping that P would occupy nitrogen sites forming isoelectronic traps and eliminating nitrogen vacancies. However, the large covalent bond difference between P and N probably prevented P from

entering the GaN crystals. Larger PH_3 pressures actually stopped the GaN crystals from growing.

There is no direct observation that nitrogen vacancies are the real cause of the high carrier density. We used catalysts such as titanium sponge in the substrate area. GaN crystals appeared to nucleate easier on the sapphire substrate under this condition, but the crystals still showed the same high carrier concentrations.

Chlorine atoms from the HCl transport species are probably not the electrically active impurities. Mass spectrometric analysis has not detected enough chlorine atoms to account for the large density of free carriers.

Lattice mismatch between the substrate and the GaN may cause local defects such as grain boundaries and dislocations. Indeed, the GaN resistivity increased with layer thickness as shown in Figure 8 and tended to saturate at higher thicknesses. However, the resistivity was still quite low, even in the thicker samples.

Single crystal GaAs, GaP, Ge, and Si were tried as possible substrates. Only polycrystalline GaN was deposited on the Ge and Si substrates. The GaAs and GaP substrates were etched away by the HCl which was used as the transport agent in the growth system.

G. Related Crystal Growth Programs

In III-V semiconductor crystal growth from the melt, vaporization of one component is usually a troublesome problem. One means of reducing the evaporation rate is to increase the total gas pressure over the melt. In order to test the effectiveness of this method, a study of the evaporation of NaCl melts as a function of pressure was undertaken in cooperation with researchers at Sandia Laboratories in Albuquerque, New Mexico.[6] The theoretical portion of the work was executed at USC. The evaporation rate of molten NaCl was measured at pressures between 0.74 and 212 psia. In induction-heated crucibles the rate was a linear function of $(1/P)^{1/3}$, with different slopes at high and low pressures. The $(1/P)^{1/3}$ dependence was shown to be expected for turbulent free-convective mass transport. Under some conditions the evaporation rate decreased with decreasing pressures. This observation was attributed to condensation of NaCl in the gas with NaCl particles being carried back into the melt by a reflux process. The large difference in evaporation rates between Ar, He, and CO_2 was
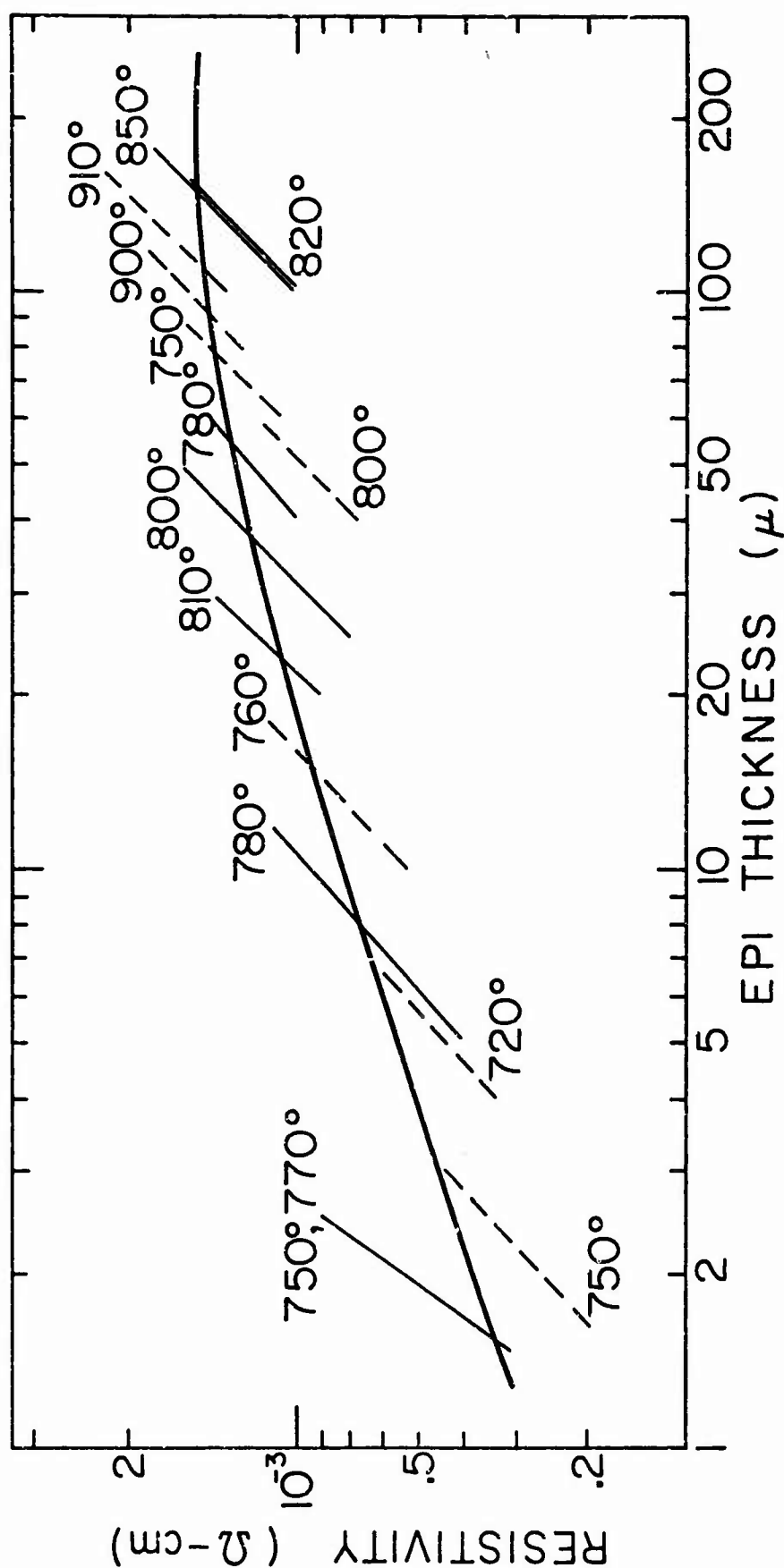
Figure 8. The GaN layer resistivity is plotted against the layer thickness. The range of the tilted lines indicates the uncertainty of the layer thickness. The dashed tilted lines are the resistivity of the runs where hot Na trap is used in the NH_3 purifications. The temperatures indicated are the substrate temperature for each run.

attributed not only to differences in thermal conductivity, but also to infrared absorption by the CO_2.

Twins are a frequent defect in semiconductor crystals, but nonetheless are of uncertain and mysterious origin. In order to improve our understanding of twin formation, twinning of KBr during solution growth was studied.[7] Large numbers of [211] penetration twins were formed when KBr reagent from one supplier was crystallized from water by evaporation. Most of these were butterfly twins, while a few were interpenetrating cubes. Some lots of reagent from another supplier also produced twins while other lots did not. The nontwinning KBr was of an overall higher purity than that which produced twins. Twin formation appeared to be stimulated by Na^+, Cl^-, and Thiazine Red R. Trace amounts of $PbCl_2$ prevented twinning. The maximum yield of twins was obtained at intermediate growth rates. The interface surface was not a twin plane, but varied widely in orientation. A model showed that the twin intersection forms a step much like that of a screw dislocation at the tip of the butterflies. Experimentally it was found that growth layers originated from this tip and later coalesced to form large waves which trapped tubular inclusions.

It has recently been shown that solvent inclusions can be made to move through a crystal by subjecting the crystal to high centrifugal fields.[8,9] (Solvent inclusions are very frequently formed in solution growth techniques, e.g., THM.) Observations of the kinetics of inclusion movement in the ultracentrifuge also provides information on interfacial processes during dissolution. We have shown that previous theoretical treatments were incorrect because they neglected dissociation into ions and electromigration of the ions in the electric field generated by the different sedimentation rates of the different ions.[10] The theory predicts a centripetal movement rate which increases as the solubility increases, which usually means as the operating temperature increases. Experimentally, the rate of movement of aqueous inclusions in potassium iodide decreased with increasing temperature and became centrifugal above about 30°C. The origin of this discrepancy between experiment and theory is unknown.

A review of mass transfer in crystal growth was published recently.[11]

H. Lapping and Polishing

Mere growth of bulk crystals is not sufficient either for characterization

or for device fabrication. Properly oriented slices with parallel damage-free surfaces are usually required. We have developed improvements over previous techniques for lapping and polishing GaAs slices. A brief discussion follows, with details available upon request.

Abrasive polishing inevitably results in a crystallographically damaged surface, although the surface may appear optically perfect. Purely chemical polishes remove damage, but generally result in rounded and/or rippled surfaces which are unsatisfactory for many applications. The best method is combined chemical-mechanical polishing. In this technique wafers are rubbed against a soft cloth, paper, or synthetic such as corfam saturated with a very slow chemical etchant. Removal rates typically range from 0.1 to 1 mil/hour. The resulting flat surface can be damage and strain-free.

Three chemical-mechanical polishing systems have been tested and improved at USC. The Syton Ⓡ system utilized a collodial suspension of ~ 25 mμ SiO_2 particles in a pH9.5 aqueous solution.[12] The surface finish produced thereby on GaAs wafers was inferior to the two other methods tested. In addition, the polishing time was longer and more abrasive pre-polishing steps were required.

The use of a solution of 0.05% bromine in methanol for chemical-mechanical polishing was first described by Sullivan and Kolf.[13] This solution emits noxious and corrosive fumes. Thus a special vented polishing apparatus was constructed of plastic. After a preliminary abrasive polish, a mirror-like surface was obtained in 1-1/2 to 2 hours. It was found unnecessary to place a light source behind the polishing wheel as recommended in Ref. [13]. In addition, the polishing wheel was horizontal, rather than inclined as in Ref. [13].

One group at USC favors the bromine-methanol polish, while others prefer our recent modification of the sodium hypochlorite (NaOCl) method of Reisman and Rohr.[14] A freshly prepared solution of 15 parts H_2O to 1 part 5% NaOCl was fed at the rate of 300 cc/hour to a Buehler polishing machine. The 8-inch O.D. wheel was covered with a Geoscience Polytex Pix polishing pad. (The polishing cloth used in Ref. [14] was rapidly attacked by the solution.) Dispensing the solutions in bursts, as in Ref. [14], was not found to be necessary. It was necessary to shut off the NaOCl solution flow and flush with water for a few minutes prior to removing the wafers in order to prevent

---

Ⓡ Registered trademark of Monsanto Chemical Co.

formation of a surface haze.

Very thin wafers for microwave device substrates are desirable both because this reduces the parasitic electrical series resistance and becau. the removal of heat is enhanced. We can now routinely prepare substrates of thicknesses down to 10 μ by use of the NaOCl chemical-mechanical process in combination with a special lapping machine which holds the wafers precisely parallel to the wheel.

I. Crystal Orientation by Cleavage Plane Reflected Laser Beam

It is frequently necessary to determine the crystallographic orientation of a nonfaceted sample of GaAs. We have developed a new and simple method for accomplishing this that does not involve X-ray techniques.[15] Reflection of a laser beam from a cleaved surface is employed. GaAs, for example, cleaves to a surface of flat mirror-like steps along {110} planes. Examination of GaAs cleaved surfaces by MacRae and Gobeli[16] with a 1000x optical microscope failed to resolve any imperfections. Electron microscope examinations showed the clevages to be flat and parallel to within the resolution of the instrument, 30 to 40 Å in height, along steps that were 3,000 to 10,000 Å in length. Step heights ranged from 50 to 200 Å. Such cleaved surfaces can be used as mirrors to reflect a well collimated light beam back upon itself. The light beam serves as one reference coordinate in a convenient space coordinate system and a cleaved plane fixes one of the crystallographic coordinates. By knowing the location of two different (110) faces and the angle between them (60° or 90°), one can locate any other plane by performing the proper rotations.

Accurate alignment, however, requires an ultra-flat face to obtain a well defined reflection. Polished surfaces, even those of a very high quality, are generally not adequate; the back reflected beam is too diffuse. A He-Ne laser (λ = 6328 Å) was used to test the flatness of typical GaAs cleavage planes which ranged in area from about 20 mm^2 to 1 cm^2. The laser was mounted on a lathe carriage so that the beam could be made to traverse the cleaved surface. The path length between the laser and the sample was 76.2 cm. Upon traversing a typical cleaved surface it was noted that the back reflected beam spot, which was 1.5 mm in diameter, never moved more than one-half of the spot diameter. This indicated that the cleavage planes in that surface were parallel to within 0.057°.

A goniometer manufactured by the Angle Computer Company, Los Angeles, was used as the crystal holder. The instrument has the ability to perform all three orthogonal rotations to an accuracy of 0.001° as read on a vernier scale. The front face of the goniometer has a machined flat which is used as a reference for the laser beam. A parallel optically flat evaporated gold mirror is placed over the machined flat. The laser beam can then be adjusted to be perpendicular to the reference plane of the goniometer to within 0.038°.

Figure 9 is a photograph of the apparatus. The crystal is mounted on a short stand-off on the optical goniometer by means of Duxseal wax manufactured by the Johns-Manville Corporation. A rough adjustment can be made by moving the crystal in the wax and by rotating the stand-off which is attached to a ball bearing. After rough alignment of the cleavage face with the laser beam, the bearing plate is tightened to hold the crystal firmly in place. Further rotation is accomplished by means of the optical goniometer itself. The laser is mounted on a microscope elevator which is in turn mounted on a jeweler's lathe carriage. The elevator has a total vertical displacement of four inches. The laser can be translated in the horizontal plane both parallel and perpendicular to the beam by adjusting the cross feed on the lathe. The maximum horizontal displacement is ten inches. Adjustment of the translational displacements is not critical, but it is important that there be no rotation of the laser during the adjustment procedure. The laser beam itself is aimed through a 2 mm hole in a flat black screen and back-reflected onto an "x" scribed 2 mm above the pinhole. The error introduced by not being able to observe the light reflected directly back onto itself is inversely proportional to the path length and is 0.15° in 76.2 cm. However, this error can be avoided by using a corrected axis which bisects the incident and reflected beams. All rotations are then performed with respect to this axis.

Transfer of the oriented crystal is accomplished by means of a precision machined plate whose longitudinal axis is parallel with the laser beam as is shown in Figure 9. The transfer plate must have the facility to be translated in three orthogonal directions so that it may be located directly under the oriented crystal. This is accomplished by mounting the plate on a Danly commercial die set modified for use as a rigid accurate elevator by inserting a threaded rod between the guide posts. The elevator is located directly in front of the goniometer. Both the elevator platform and the transfer plate have
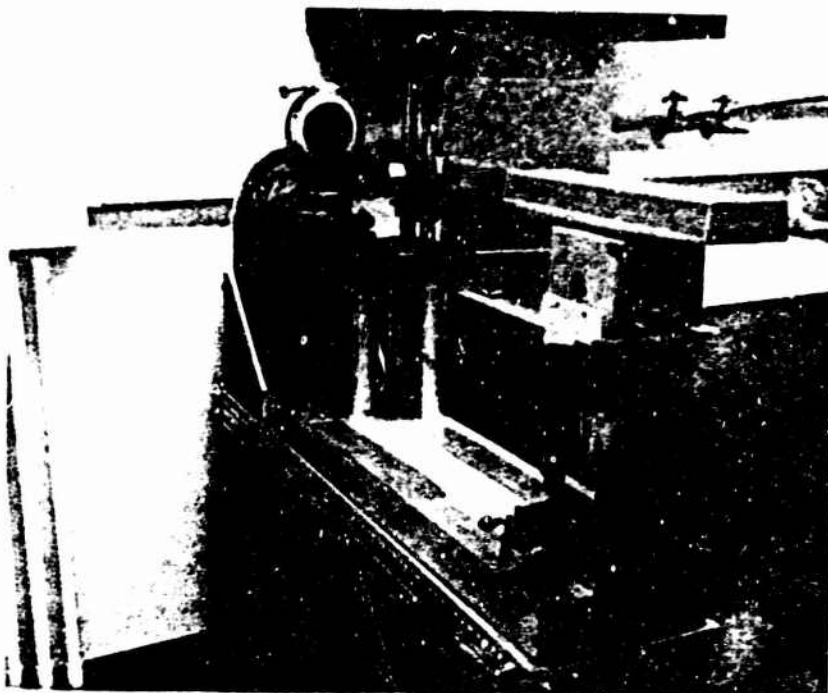
Figure 9. Crystal orientation apparatus using cleavage plane reflected laser beam.
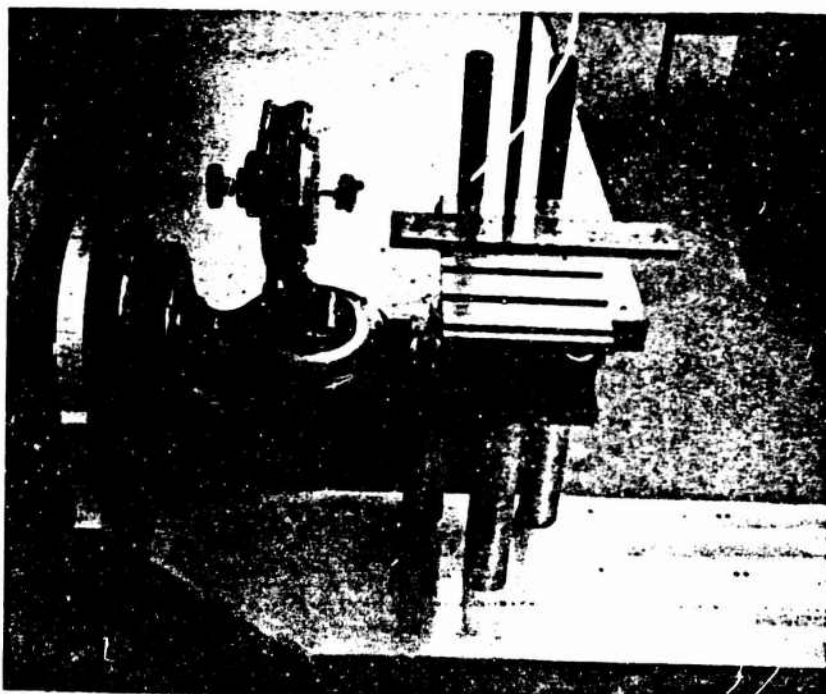
Figure 10. Optical goniometer and transfer assembly.

14 - A

longitudinally cut steps as shown in Figure 10. These mating steps allow the plate to slide in a direction parallel to the laser beam and move by steps perpendicular to the beam. The plate is aligned such that its longitudinal axis is parallel to the laser beam. The entire assembly (laser, optical goniometer, and transfer device) is mounted on a 10" x 2-1/2" x 48" aluminum channel which is fastened to a steel table with provisions for leveling and vibration damping.

After orientation, the crystal is rotated 90° with respect to the laser beam such that its oriented face is now parallel with the longitudinal edge of the transfer plate. Plaster of paris is used to attach the crystal to the transfer plate and the wax is removed after the plaster sets. The plate with the oriented crystal can then be transferred directly to a magnetic chuck wafering machine. A lip has been accurately machined on the transfer plate for alignment with the magnetic chuck.

The system is a compact, simple laboratory tool which is quick and easy to use. A crystal may be oriented in less than five minutes and the transfer time is only dependent on the media used for adhesion (20 minutes for quick setting plaster of paris). The possible errors due to the transfer procedure are misalignment of the transfer plate, misalignment of the saw chuck, and walking or wobble of the saw blade. All of these errors compounded, however, are less than 0.15° error due to off-axis back reflection of the laser beam. The orientation of slices wafers has been checked by Bragg diffraction and found to always be within the accuracy of the X-ray machine, 0.20°.

J. Contacts and Heat Sinks

Fabrication of any semiconductor device ultimately requires reliable metal contacts to portions of the semiconductor. Reproducible formation of reliable contacts to GaAs appears to have been particularly elusive. We have developed a new technique yielding specific contact resistances as low as $\sim 1 \times 10^{-5}$ ohm cm^{-2} (for GaAs with $n = 1 \times 10^{18}$ cm^3). The contacts are ohmic for electron concentrations in the GaAs of $< 10^{13}$ cm^{-3}. They can be made by sputtering of tin or by a relatively simple short circuit electro-plating of tin from a $SnCl_2$-KCl-NH_4Cl salt bath on GaAs previously electro-plated with gold. The other electrode of the molten salt short circuited cell is a Au-Sn alloy with the composition desired on the Au plated GaAs. It has been demonstrated that the average Au-Sn alloy compositions can be easily

regulated to within 2%. One can thermocompression (TC) bond Au wires to these contacts. Required alloy temperatures are relatively low, 350-375°C.

A new method has been developed for assuring intimate contact between a device and a heat sink. It is applicable to Gunn devices, avalanche diodes, etc. A copper heat sink is electroplated onto the entire semiconductor slice. Diodes are fabricated by etching from the reverse side. Individual diodes are separated by sawing the copper into small squares.

For heat sinks or mechanical support, a thick metal layer is frequently desired. To have good thermal conductivity and to be strain-free, the metal must be free of organic or chemical inclusions. We have developed a new copper electroplating technique which accomplishes this. Prior to plating a metal film is deposited by vacuum evaporation. The first metal layer is selected for good ohmic contact and adhesion. The top layer is gold approximately 4000 Å thick. After wax mounting a 0.3 to 0.5 mil layer of gold is electrodeposited from a 24 karat neutral bath. A copper lead wire is attached to the gold surface. Copper is plated from a fluoborate bath without additives or from an acid bath. Temperature is 54 to 71°C and current density 1/2 to 1 ma/cm^2.

II. CHARACTERIZATION

A. Dislocation Studies

Dislocations are introduced during crystal growth and are known to influence the semiconducting properties of the crystal. Unfortunately, a great deal is unknown both about dislocation generation during growth and about their electrical effects. Therefore we are studying dislocation structures in as-grown and in deformed crystals, and their influence on electrical properties.

1. Characterization of A(111) and B($\bar{1}\bar{1}\bar{1}$) Surfaces of GaAs by Etching

GaAs belongs to the class of $A^{III}B^{V}$ semiconductor compounds which crystallize in a noncentrosymmetric zincblende lattice. Because this structure contains a polar axis it is customary to designate the {111} plane consisting of Ga atoms as the A(111) surface and the ($\bar{1}\bar{1}\bar{1}$) plane of As atoms as the B($\bar{1}\bar{1}\bar{1}$) surface. There are also two types of edge dislocations: α, when the extra half-plane of the dislocation ends on a row of Ga atoms, and β when the plane ends on a row of As atoms. Since different electrical and chemical properties are associated with these two types of surfaces, it is highly important, therefore, in the characterization of GaAs to be able to identify these two planes and two types of dislocations. As described below, we have studied etching methods for displaying the features of the A(111) and B($\bar{1}\bar{1}\bar{1}$) surfaces of GaAs.

A GaAs sample grown by a horizontal Bridgman technique was oriented along the <111> direction using standard Laue X-ray back-reflection methods. Wafers (3 mm x 10 mm) were slices parallel to the (111) Bragg plane. Both top and bottom surfaces of the wafers were lapped on the plate glass in a slurry of 3200-micron powder. Surface damage was removed by immersing the samples in a chemical polishing solution consisting of one part HF, three parts HNO_3 and two parts H_2O.[17] The resulting thicknesses ranged from 0.1 to 0.8 mm.

The samples were separately etched in three different solutions[17] to reveal dislocation pits on either or both A(111) and B($\bar{1}\bar{1}\bar{1}$) surfaces. The density of these pits was calculated from several samples and from several areas of the same sample. The dislocation densities, chemical composition of the etchants and suitable etching times are listed in Table 2.

The photomicrographs of the A(111) and B($\bar{1}\bar{1}\bar{1}$) surfaces etched by the three solutions are shown in Figures 11 through 13. Figure 11 shows that by using the first etchant (Schell reagent), dislocation pits appear only on the
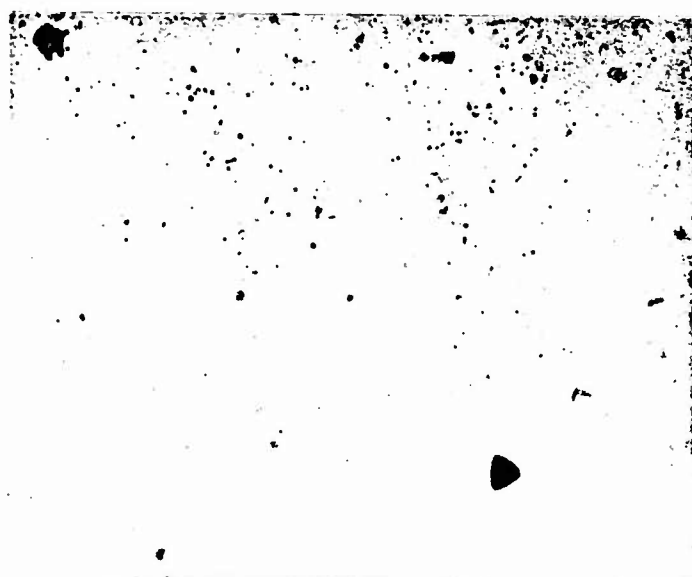
Table 2

Dislocation Densities and Etchant Data for GaAs A(111) and B($\bar{1}\bar{1}\bar{1}$) Surfaces

Etchant No.	Etchant Composition and Etch Time	Dislocation Density, ρ (in cm^{-2})			
		A (111) Surface		B($\bar{1}\bar{1}\bar{1}$) Surface	
		Sample	ρ	Sample	ρ
1	Schell's Reagent: 1 - Part HNO$_3$ 3 - Parts H$_2$O	E1	0.6×10^4		
		E1-A	2.0×10^4 0.8×10^4 1.0×10^4 5.0×10^4		—
	15 minutes @ 80°C (Sample E1)	Average	1.9×10^4		
2	Schell + 0.5% Butylamine	E2-A	1.0×10^4	E2-B	4.3×10^5
		E2-C	1.2×10^4 2.8×10^4 1.1×10^4	E2-D	1.0×10^4 2.0×10^4
	15 Minutes @ 26°C (Sample E2-A) 25 Minutes @ 26°C (Sample E2-B)			E2-E	0.4×10^4 0.5×10^4
		Average	1.3×10^4	Average	1.6×10^4
3	Schell + 0.5% AgNO$_3$	E3	1.2×10^4	E3	1.3×10^4
		E3-A	1.9×10^4 3.8×10^4	E3-A	3.0×10^4 6.0×10^4 0.2×10^4
	15 Minutes @ 80°C (Sample E3)	Average	2.3×10^4	E3-B	0.5×10^4 7.0×10^4 2.0×10^4
				Average	2.8×10^4

a. A(111) surface   200X
    Sample E1   No. 011

b. B($\bar{1}\bar{1}\bar{1}$) surface   200X
    Sample E1   No. 025

18-A

Figure 11. Dislocation etch pits resulting from use of Schell's reagent
            on A(111) surface of single crystal GaAs. No etch pits
            appear on the B($\bar{1}\bar{1}\bar{1}$) surface.

A(111) surface but not on the B($\overline{1}\overline{1}\overline{1}$) surface. This designation of surfaces relative to etching behavior was established by other investigations for other $A^{III}B^V$ compounds.[18] The A(111) surface of sample E1 was characterized by well defined tetrahedral pits (Figure 11-a), while pits with defined geometrical shapes were not observed even at higher magnifications (up to 1000X) on the bottom or B($\overline{1}\overline{1}\overline{1}$) surface of the same sample.

The absence of dislocation pits on the B($\overline{1}\overline{1}\overline{1}$) surface has been attributed to the sensitivity of the B($\overline{1}\overline{1}\overline{1}$) surface to the dissolving power of Schell's reagent. By adding an inhibitor, butylamine (or amylamine) to Schell's reagent, etch pits were revealed on both A(111) and B($\overline{1}\overline{1}\overline{1}$) surfaces as shown in Figure 12. While the etch pits on the A(111) surface of sample E2-A (Figure 12-a) were found to be similar in shape and size to those found in sample E1 (Figure 11-a) and observed at a lower magnification, the etch pits on the B($\overline{1}\overline{1}\overline{1}$) surface of sample E2-B were found only at higher magnification and after longer etching times (Figure 12-b).

It was suspected, however, by other investigators that the second etchant revealed on the B($\overline{1}\overline{1}\overline{1}$) surface only a portion of the total number of dislocations actually present.[17] Hence, a third etchant (Schell + 0.5% AgNO$_3$) was applied to both surfaces of sample E3. Figure 13 shows the dislocation etch pits resulting from the use of this third etchant. On the A(111) surface, conical pits instead of the tetrahedral pits shown in Figures 11-a and 12-a became visible (Figure 13-a). On the B($\overline{1}\overline{1}\overline{1}$) surface of the same sample, E3, tetrahedral pits are shown (Figure 13-b) with initial signs of overetching. Thus the tetrahedra appeared to break up into smaller rectangular parallelipipeds which were observed in earlier micrographs. Because these rectangular features might be mistaken for etch pits, Figure 13-b can be used as a guide when estimating the density of dislocations revealed by this etchant.

The three etchants may be characterized by the types of dislocations revealed on either surface. On the A(111) surface, all three etchants reveal both α and β dislocations (Ref. 17) so that the dislocation densities on the three A(111) samples should be about the same. Table 2 shows that the average dislocation densities are within the same order of magnitude.

While the first etchant (Schell's reagent) failed to reveal any dislocation pits on the B($\overline{1}\overline{1}\overline{1}$) surface (Figure 11-b), the second etchant (Schell + 0.5% butylamine) revealed what are believed to be α-dislocations, subject to further verification by the bending experiments described later. The third

a. A(111) surface   200X
   Sample E2-A   No. 015

b. B($\bar{1}\bar{1}\bar{1}$) surface   500X
   Sample E2-B   No. 025

19-A

Figure 12. Dislocation etch pits resulting from use of Schell's reagent
            + 0.5% butylamine.

a. A(111) surface   200X
   Sample E3   No. 013

b. B($\bar{1}\bar{1}\bar{1}$) surface   200X
   Sample E3   No. 014

19-B

Figure 13. Dislocation etch pits resulting from use of Schell's reagent
            + 0.5% AgNO$_3$.

etchant (Schell + 0.5% AgNO$_3$) is known to reveal both α and β dislocations, so that the dislocation densities observed in the third sample (Figure 13-b) should be higher than those found in the second (Figure 12-b). Table 2 shows that such is the case although the differences in dislocation densities observed in samples E2 and E3 were not as large as those reported by other workers.[17]

2. Studies of GaAs Crystals by X-ray Topography

We have studied the dislocation structure of our as-grown GaAs crystals by X-ray topography. The use of this technique is important since the etching technique is limited to the identification of etch pit sites on major crystallographic planes with emergent dislocations. Furthermore, the reliability of the estimates of dislocation density depends upon the particular etchant employed on the opposite faces of GaAs crystals, as just described. The action of etchants on α- and β-type dislocations on both (111) and ($\bar{1}\bar{1}\bar{1}$) faces is still not entirely clear.

In past years, because of the high X-ray absorption of GaAs crystals, X-ray investigations were commonly carried out by the anomalous transmission method. Since we are now able to prepare and handle very thin slices of GaAs crystals, transmission Lang topographs are possible. In this method the diffraction geometry is simpler and more reflection planes can be studied.

GaAs wafers were usually sectioned along (111) planes and lapped and chemically polished down to 50 μm by the techniques described in Section I.H. In most cases, X-ray topographs of {111}, {202} and {422} reflections were studied. Illustrated in Figure 14-a is a ($\bar{2}4\bar{2}$) topograph of a section of GaAs grown by the horizontal Bridgman technique taken from our new Kristallos X-ray topographic camera with Mo Kα radiation. For such a crystal, several types of imperfections can be illustrated. The dislocation density in the central region was rather high (estimated $\sim10^4$), and individual dislocations were difficult to resolve. Low dislocation densities were found along the edges of the crystal. Dislocation loops were also found in our crystal. It is particularly interesting to observe the spiral image located near the center of the crystal. This could be a result of a screw type growth defect. Figure 14-b is a ($\bar{2}42$) topograph shown at a higher magnification (20X). It is clear that dislocation loops and scattered dislocations were more abundant in the adjacent region. The majority of dislocations in the central region are aligned in the
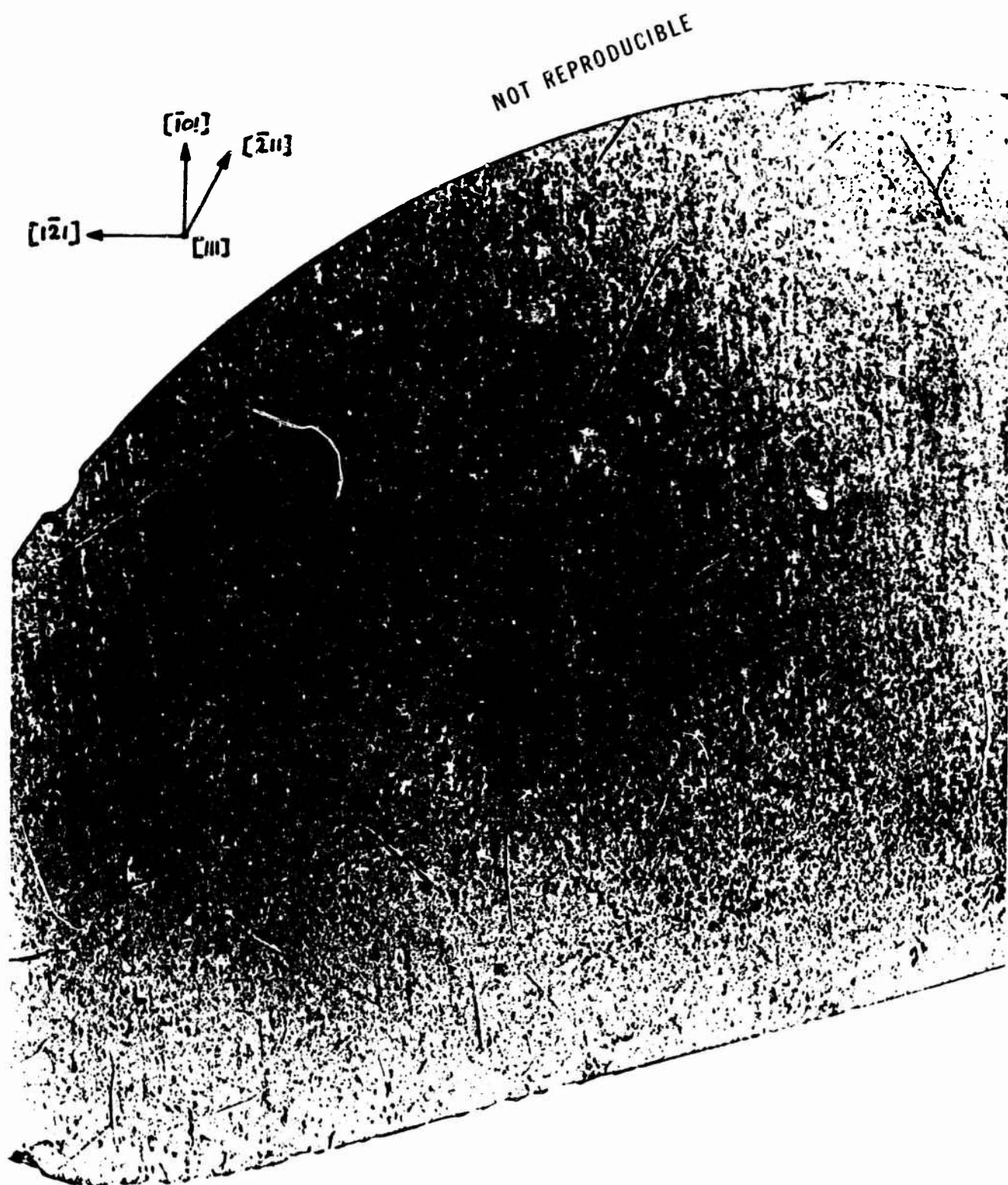
Figure 14a. ($\bar{2}4\bar{2}$) transmission Lang topograph of a (111) wafer cut from a horizontal Bridgman-grown GaAs crystal (X10)
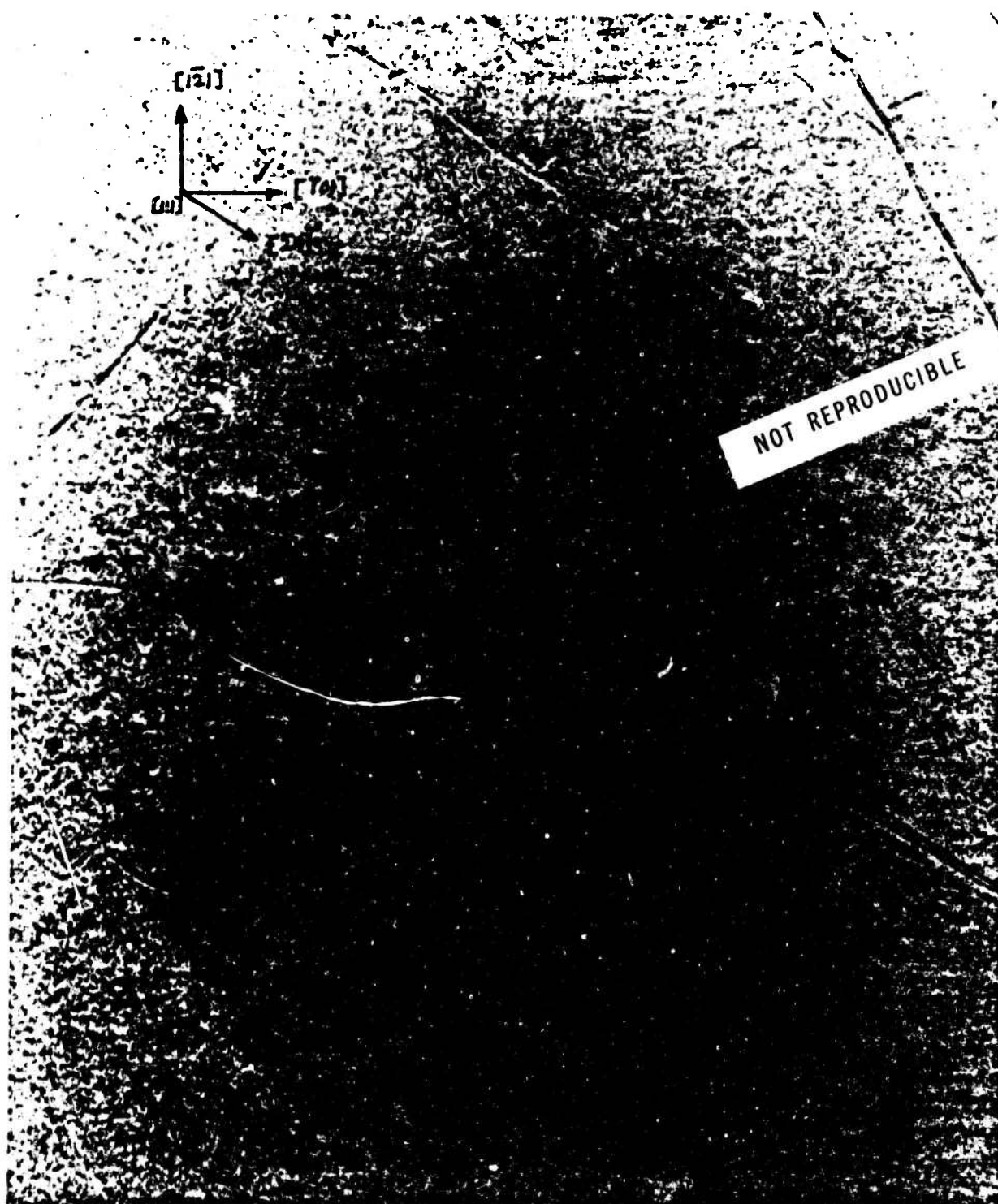
Figure 14b.   ($\bar{2}$42) topograph of the crystal in Figure 4a. (X20).

<110> direction. The points with black and white contrast represent segregation of impurities (oxides or Ga inclusions).

3. Plastic Deformation of GaAs Crystals

A four-point bending jig was designed in order to introduce a uniform distribution of dislocations of particular type (α or β) for the study of their influence on the transport properties and to elucidate the mechanisms generating dislocations during growth. The bending jig has been modified so that both direct and indirect heating of the specimen can be performed in the same unit. We have found that indirect heating of the crystal inside a small heating chamber is superior to direct joule heating of the crystal by an electric current. A typical bent crystal and its dimensions are shown in Figure 15. Both etch pit and X-ray methods have revealed a large increase in dislocation density. Several doped and undoped GaAs crystals have been prepared and their electrical properties are being measured. In addition to measurements at USC, Dr. Wieder at the U.S. Naval Electronics Laboratory in San Diego has offered to make Hall, photoconductive, photovoltaic, and Gunn-effect measurements on our samples before and after bending.

B. Glow Discharge Spectroscopy for the Analysis of Thin Films

We have investigated flow discharge spectroscopy (GDS) as a method for trace analysis of thin films. In this technique, the target is sputtered in a low pressure gas discharge. The discharge is operated in the abnormal glow mode and its spectra is monitored for the electroluminescence associated with the desired sputtered target elements. Under suitable conditions, the intensity of the spectral line of an element in the target is proportional to the density of that element in the region of the discharge under observation.

The presently available methods for trace analysis which may be applied to thin films are limited primarily by the small volume of sample available. Typical dimensions of the GaAs thin films used in the following experiments are 0.7 to 10 µm in thickness by 0.3 to 0.5 cm^2 in area. For a sample volume of 4×10^{-5} cm^3 and an impurity concentration of 10^{17} atoms cm^{-3} there are only 4×10^{12} total impurity atoms available for analysis. If the dopant is a heavy metal such as Sn, the total mass of impurity atoms is 7×10^{-10} g.

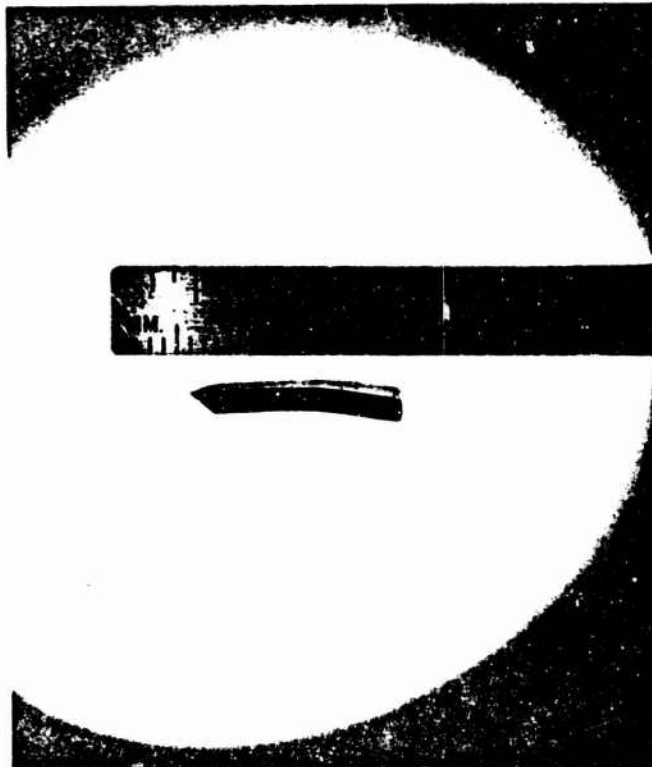Figure 15. A GaAs crystal after bending around a <112> axis at 700°C. The (Ī11) slip planes are at 45° to the crystal surface.

The use of sputtering as a means for atomizing the sample offers several distinct advantages. The etch or depth removal rate can be varied over a wide range (0.01 μm/min. to 10 μm/min.). No surface preparation of the sample is required. Sample contamination is not a problem since the film does not have to be chemically dissolved in a solvent. Most importantly, sputtering is basically a process which "etches" the sample in an "atom by atom" fashion. The discharge associated with sputtering in the abnormal glow regime provides a controllable source of excitation for sputtered atoms. DC sputtering is convenient for metals and semiconductors, whereas RF sputtering can be used for insulators.

Figure 16-a shows the plan view of the sputtering module. The module itself is pyrex glass with the exception of the window which is G.E. type 151 UV transmitting quartz. The anode and cathode are aluminum and are water cooled. A grounded cylindrical aluminum sputter shield fits over the cathode. The sputter shield and cathode are insulated by means of a quartz sleeve and a delrin plastic spacer with delrin screws. All vacuum seals are made with viton O-rings. Details of the cathode assembly are indicated in Figure 16-b.

The cathode-anode gap distance can be adjusted by sliding the anode through a modified Veeco C-112 vacuum quick disconnect. Spacing screws allow the distance to be adjusted to within 0.5 mm. The target sample is mounted with silver paste on a demountable aluminum pedestal which screws into the cathode. Pyrex shields are used to mask any exposed aluminum on the cathode assembly from the plasma. This prevents arcing between the pedestal and the grounded shield. It also prevents sputtering of the pedestal. The gas inlet was placed next to the window to minimize the deposition of sputtered material on it.

In operation, the system is purged several times with argon gas and pumped down to a pressure of less than 10^{-3} torr with a rotary vane pump. The outlet line from the sputtering module is isolated from the mechanical pump by a liquid nitrogen cold trap. Ar used in these experiments had an initial purity of 99.998%. It was passed through a quartz trap containing titanium sponge at 900°C to remove traces of O_2, N_2, hydrocarbons, and water vapor. After the initial pump down, the operating Ar pressure of 0.1 torr was maintained by bleeding the purified gas into the pumped module at an approximate rate of 0.5 cm^3 atm/min.

A voltage is established between the cathode and the anode which ionizes
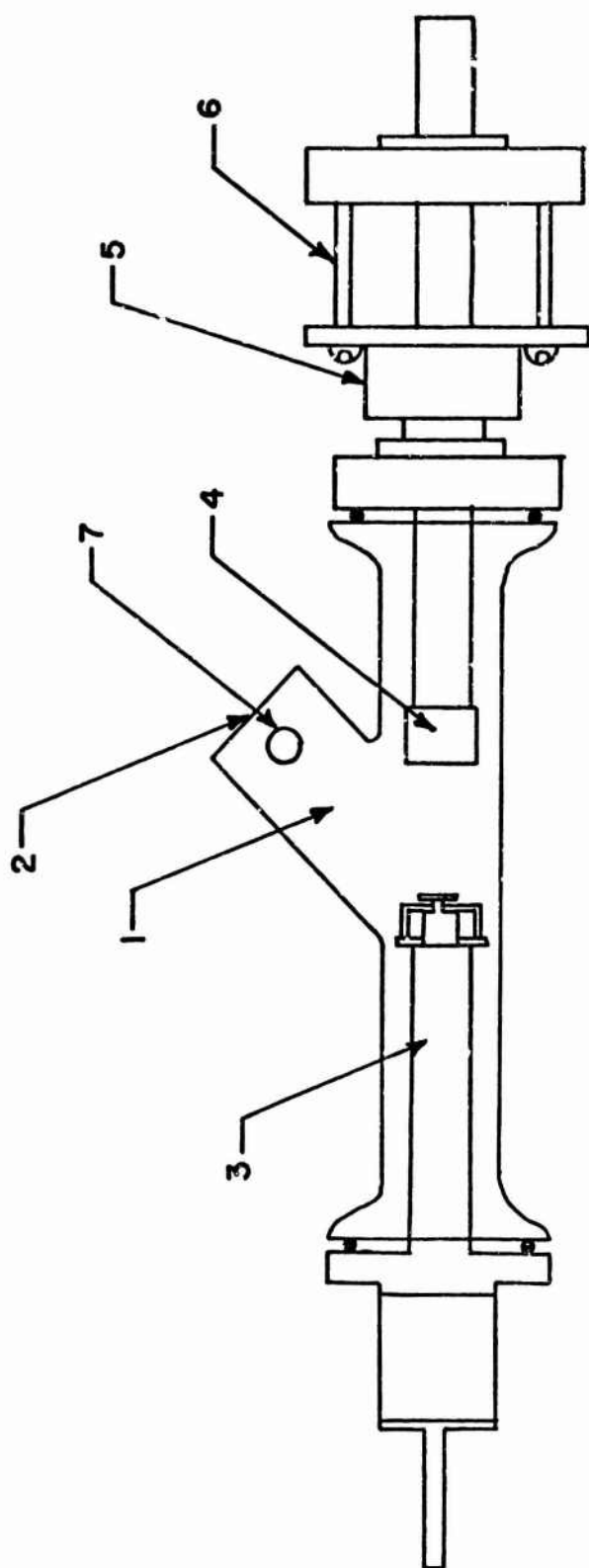
Figure 16a. Plan view of sputtering module:
(1) pyrex module, (2) quartz window,
(3) aluminum cathode, (4) aluminum anode,
(5) modified Veeco C-112 vacuum quick disconnect,
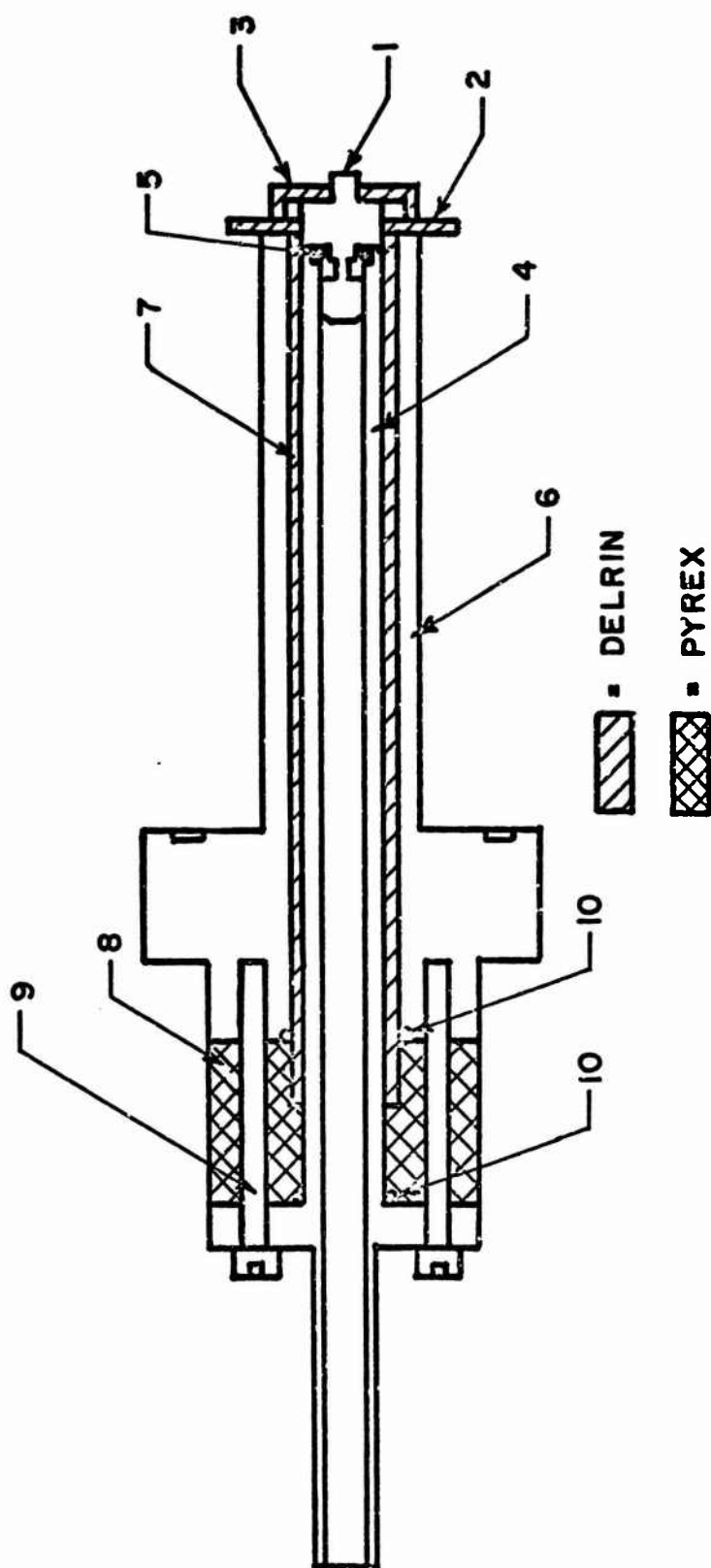(6) spacing screws, and (7) gas inlet.

DELRIN

PYREX

Figure 16b. Cross-sectional view of cathode assembly:
(1) sample holder, (2) pyrex shield, (3) pyrex shield,
(4) cathode, (5) Viton O-ring, (6) aluminum sputter shield,
(7) pyrex sleeve, (8) delrin insulator, (9) delrin screws,
and (10) Viton O-ring.

22-B

the gas and accelerates the Ar ions which bombard the target. Target atoms are ejected primarily in their neutral ground states and are subsequently excited in the plasma. As shown schematically in Figure 17, the electroluminescence is focused by a set of mirrors, chopped at a frequency synchronous with a phase sensitive lock-in amplifier, monochromaticized by a scanning spectrometer, and detected by an EMI 6256S photomultiplier. The 1200 groove per mm grating in the spectrometer was blazed for a wavelength of 2000 Å. The f number of the spectrometer was f3, but the geometry of the mirrors was such that the effective f number of the optical system was f16. The amplified signal was recorded as either intensity versus wavelength or intersity versus time.

Experiments were performed to determine in which region of the discharge the maximum target atom electroluminescence occurs. A module with the snout perpendicular to the cylindrical axis was used. Two alignment slits were placed between the module window and the plane mirror. Using this arrangement, the lignt incident upon the spectrometer slit originated from a narrow slice of the discharge. The module was mounted on the tracks of an optical bench so that it could be translated in a horizontal plane perpendicular to the spectrometer slit. This permitted the spectra to be examined as a function of distance between the electrodes. Figure 18 shows the neutral 2860.4 Å line intensity as a function of distance from the GaAs target. The smaller slope on the left side of the maximum is due to the discharge geometry. The maximum intensity occurs in the cathode glow region at approximately 2.5 mm from the target surface. Calculations also showed that this is the region in which the ejected target atoms have experienced enough collisions to have given up their initial ejection kinetic energies. In these calculations the mean free path for a "hot" atom in a thermalized gas was used. The ejection energies were estimated from the work of Stuart, et al.[22,23] Elastic collisions and random walk isotropic scattering were assumed, although a correction was made for the "persistence" of velocity.[24]

Knowledge of the intensity distribution in Figure 18 provided the basis for selecting the analysis module shown in Figure 17. This module configuration insured that the measured electroluminescent intensities were independent of minor uncertainties in alignment. The use of glow discharge spectroscopy for chemical analysis requires that the luminescent intensity due to a particular
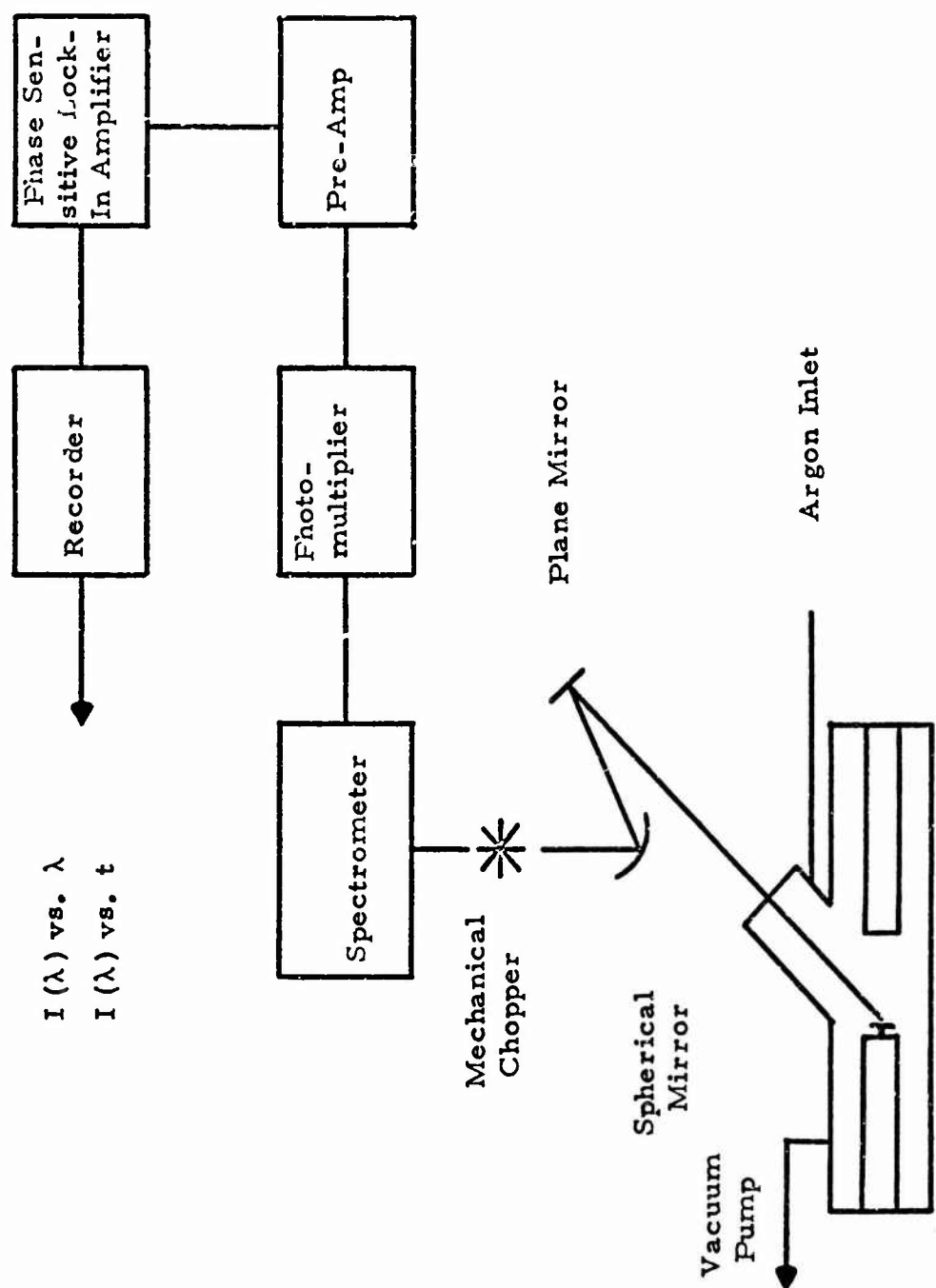
Figure 17. Schematic diagram of the optical and electronic detection system.
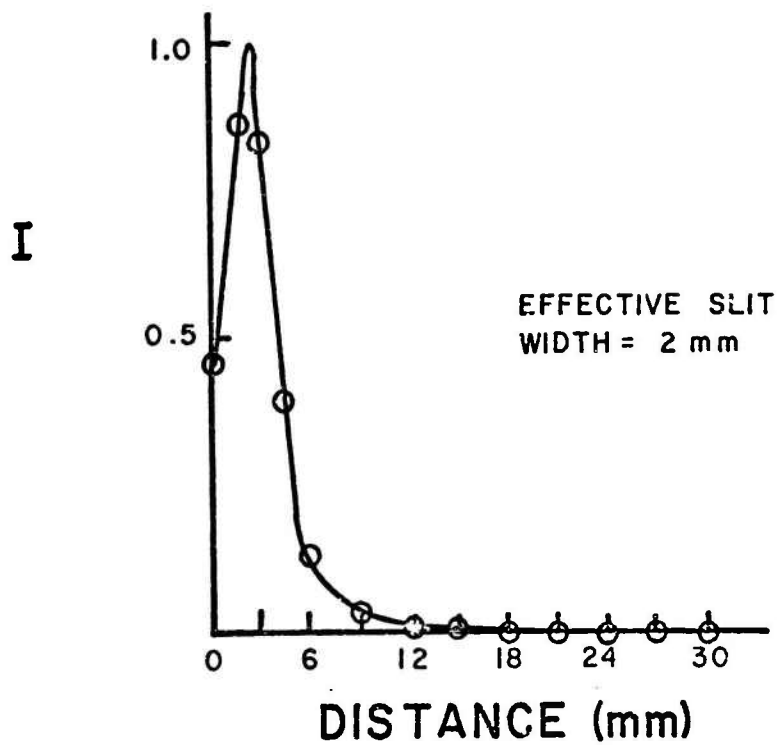
Figure 18. Target atom emission intensity (arbitrary units) versus distance between target and anode.

target constitutent be proportional to the sputtering rate. That this is indeed the case was suggested by the prior work of Stuart and Wehner.[25,26] To establish this proportionality we measured the relative spectroscopic yield curves for several GaAs orientations and established that these could be normalized with absolute yield data. Yield curves were measured for the following orientations: (111)Ga, (111)As, (110), and (211). All samples used were single crystals with chemically polished planes corresponding to one of the above orientations.

The spectroscopic yield is presently defined as the emission intensity measured in arbitrary units divided by the cathode current. The emission intensity was monitored for transitions from neutral excited states to neutral ground states. The relative yield curves for all orientations mentioned above were measured and checked using both Ga and As lines at 2874.2 Å and 2860.4 Å, respectively. Data points were taken at intervals of 50 or 100V and the results are summarized as the solid curves in Figure 19.

Each curve in Figure 19 was normalized with an absolute yield measurement and the normalization checked with other absolute yield data. Absolute or mass yield is defined herein as the number of target atoms sputtered per second per unit of cathode current in electronic charges per second. This definition of mass yield is identical to the usual one, the number of target atoms ejected per incident Ar^+ ion, if current contributions by secondary electrons and multiply-charged ions are neglected. These current components are less than 20% of the total. Absolute measurements were made using the "change in mass" technique as discussed in detail by Kaminsky.[27] The absolute yield data are indicated by circles in Figure 19. The normalized spectroscopic yield curves agreed to within 6% of the absolute yield data. These results established the proportionality between the sputtering rates and the luminescent intensities. The yield curves proved to be highly reproducible and served as a sensitive monitor of the sputtering rate. Errors in the absolute yield measurements are estimated to be less than 3%.

From Figure 19 it can be seen that the sputtering yield varies as the crystal transparency,[28,29] i.e., the number of atoms per unit area in a plane normal to a particular direction. The more tightly packed planes exhibit higher sputtering yields. Channeling effects[30] may also play some role, especially at the higher energies. A polarity effect is evident in the (111)
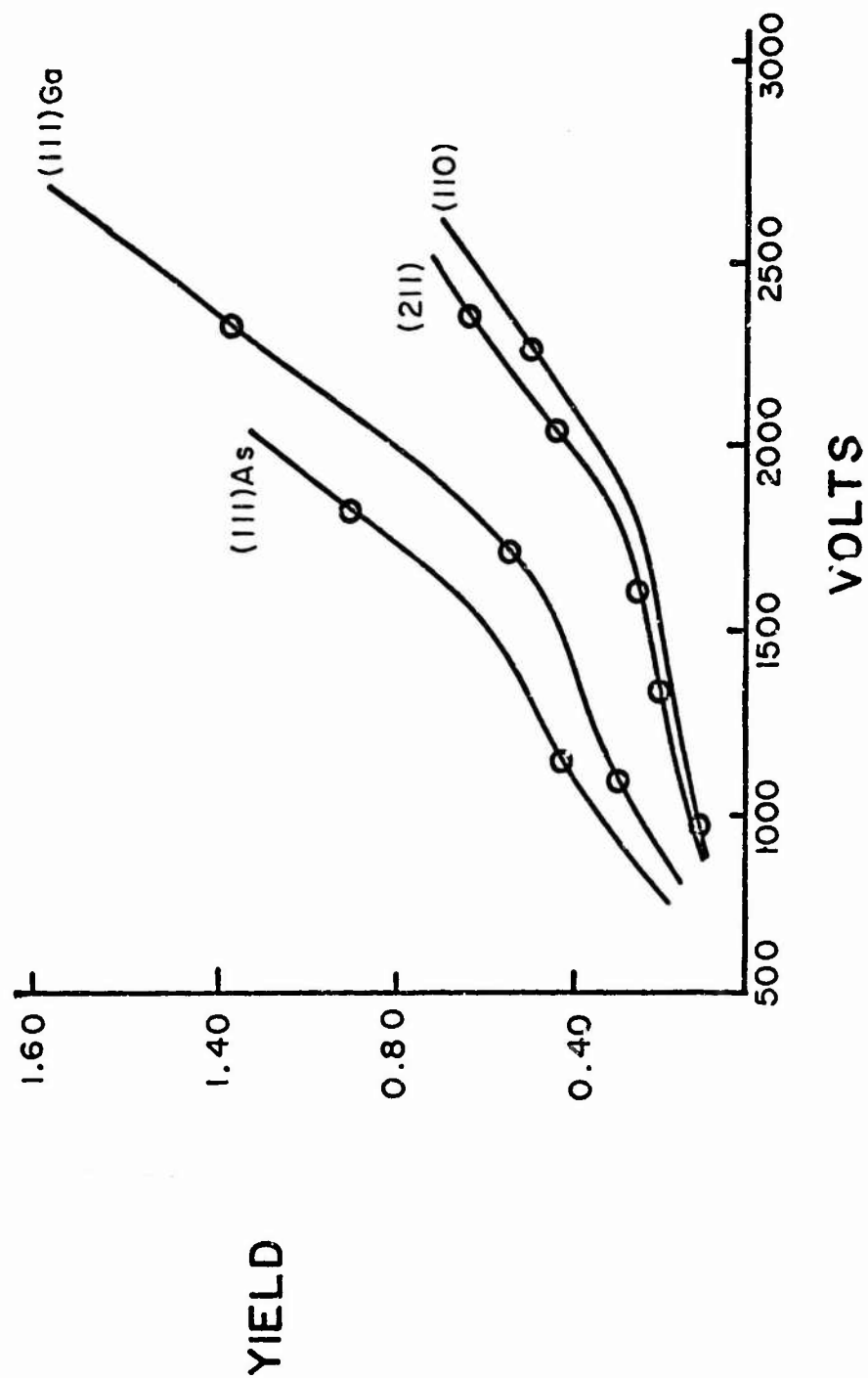
Figure 19. Sputtering yield (target atoms sputtered per unit of cathode current) versus applied voltage for different orientations of GaAs.

24-A

planes. The (111) As plane sputters faster in agreement with chemical etching work done by Gatos and Lavine.[31] These authors showed that the As face is the more reactive with respect to chemical etches. In addition, there is a change in the energy dependence of the yield function between 1300 and 1700 V. The knee in the yield curve occurs at lower energies for planes with higher sputtering rates.

Tin was selected as the main impurity to be studied in GaAs for three reasons: (1) it has a high emission intensity in a copper art;[32] (2) it is an important dopant in GaAs, and (3) the tin peak at 2849 Å occurs in a spectral region in which Ar is fairly transparent, thereby minimizing background intensity problems. Figure 20 shows two superimposed spectra that were taken to establish the detection limit for Sn in GaAs. The solid curve is the spectra for a GaAs sample containing 9×10^{17} Sn atoms cm^{-3} and the dotted line is for a GaAs sample containing no Sn. Both samples had the same area and they were sputtered under the same conditions. The spectral resolution was better than 1 Å. All peaks not labeled, including the shoulder peak at 2841 Å on the Sn line, are due to Ar. Variations in the background intensities of the Ar spectral peaks are less than 10% from one run to another. Within these limits the observed Sn emission line can be corrected for the Ar background. The concentration of Sn in a given GaAs sample is estimated by comparing the intensity of the Sn line with that of a GaAs standard containing a known amount of Sn. For each sample the Sn line intensities are measured in units of either a Ga or As peak intensity which is highly reproducible as indicated by the repeatability of the yield curves.

The current detection limit for Sn in GaAs was estimated from the spectra in Figure 20 and the sputtering conditions, i.e., a sample area of 0.38 cm^2 and a sputtering rate of 0.07 μm/min. The detection limit was conservatively selected as the Sn concentration for which the intensity of the Sn peak is equal to that of the Ar shoulder peak at 2841 Å. Sn can be detected at lower levels, but the reproducibility is less. Using this definition of detection limits, the minimum weight of Sn that can presently be detected is 7×10^{-10} g. The minimum concentration of Sn that we can detect is 3×10^{16} atoms cm^{-3}. This is for a sample with an area of 0.5 cm^2, a thickness of 2.0 μm, and a sputtering rate of 0.3 μm/min. A Sn concentration of 9×10^{17} atoms cm^{-3} can be detected in a GaAs film only 0.7 μm thick with a surface area of 0.4 cm^2. The reproducibility of
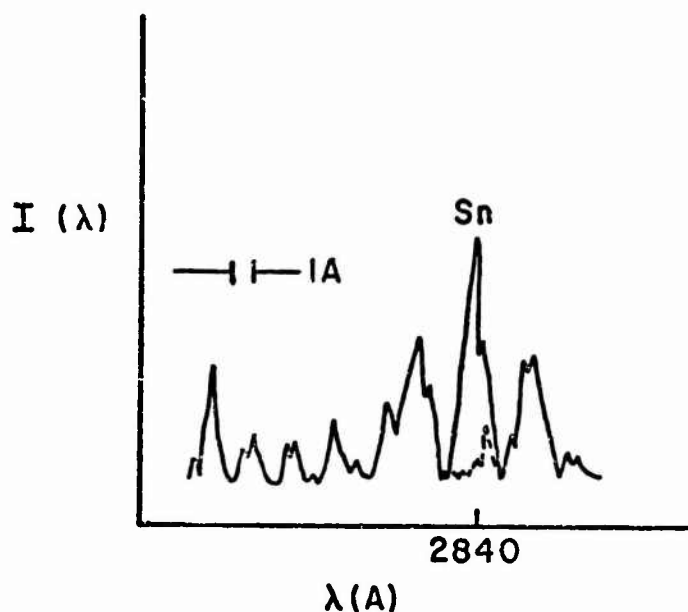
Figure 20. Emission intensity versus wavelength from the cathode glow portion of the discharge for two superimposed spectra. The solid line corresponds to a GaAs sample containing 9×10^{17} atoms cm^{-3} of Sn, the broken line is the spectra for a GaAs sample containing no Sn.
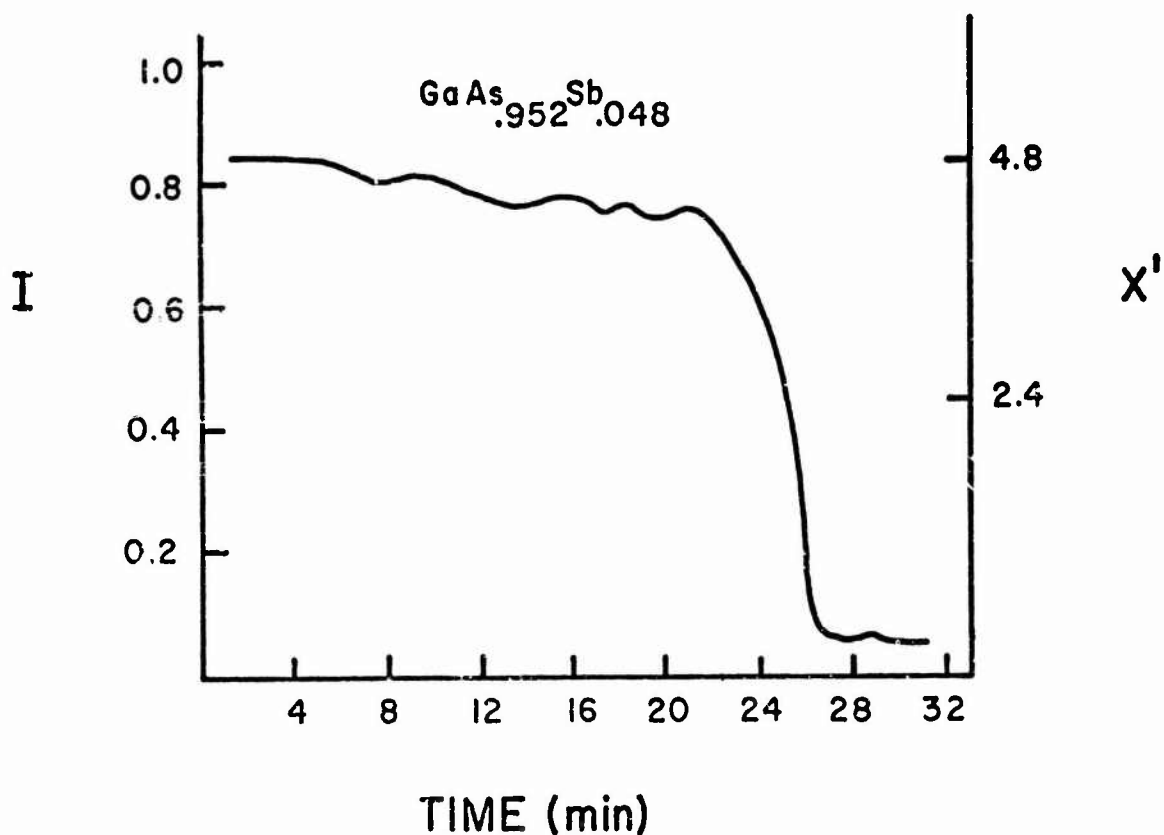

TIME (min)

Figure 21. Emission intensity (arbitrary units) of the 2598 Å Sb line as a function of time. Target was an epitaxial GaAs$_{.952}$Sb$_{.048}$ film on a GaAs substrate. x^1 is the relative mole fraction of Sb.

all of these measurements is within 10%.

In addition to Sn, the following elements have also been detected: Ga, As, Sb, Al, Si, and Cu. Detection limits have not been established for these elements. Estimated limits are $\sim 5 \times 10^{17}$ atoms cm^{-3}.

The sensitivity of GDS can be increased by increasing the number of electrons in the plasma available for excitation. Two possible methods for achieving this are the use of a transverse magnetic field or a hot filament. However, both of these methods cause non-uniform sputtering. Another possibility is to use a coherent light source of the proper wavelength for exciting the desired impurity. Lasers are becoming increasingly more available in the UV. However, light scattering may cause problems and would have to be considered.

The use of different sputtering gases should also be studied for two reasons. First, one should select a gas which is as transparent as possible in the spectral region of interest. Secondly, one should consider gases with low ionization potentials to increase the number of free electrons available for excitation. The use of Xe (which has a lower ionization potential than Ar), mixtures of rare gases, and specialty gases such as those used in nuclear detector tubes should be considered. However, care must be taken to choose a gas which does not react with the target species in the gas phase to produce species with lower emission intensities. Additives to a rare gas must also not form undesirable masking deposits on the target during sputtering.

Another application for GDS that we have investigated is the concentration profiling of alloy thin films. This technique can be used to estimate the concentration of the constituents as a function of depth through the alloy film. Figure 21 shows a scan that was made while monitoring the Sb concentration in a GaAs$_{.952}$Sb$_{.048}$ film. The film was grown on a (111)As-oriented GaAs substrate and was about 10 μm thick. The sputtering rate was 0.3 μm/min., and the intensity of the Sb line at 2598 Å was monitored. The upper plateau is flat to within 10%, i.e., $\Delta x \leq 0.1$ x where x is the relative mole fraction of Sb. This indicates that the distribution of Sb is homogeneous to within 10% which is consistent with X-ray line broadening and photoluminescent measurements reported by C. T. Li.[33] The variation is also within the range expected from the alloy growth conditions.

The depth of sample over which one can observe a meaningful change in the Sb concentration is limited primarily by the sputtering rate and the time

constants of the amplifiers. In this case the depth resolution is about 0.2 μm.
The sputtering rate of the above alloy film was found to be a factor of two
less than that of (111)As-oriented bulk GaAs. The reason for this is not
obvious to us.

The variations in the upper plateau of Figure 21 are greater than expected
from background noise. They correspond to either small changes in the sputtering
rate or inhomogeneities within the film. After the profile was taken, the GaAs
substrate was sputtered under the same conditions except that this time the Ga
line was monitored. The intensity response was flat to within 1% over the
same length of time. In future alloy profiling experiments we intend to
monitor the sputtering rate directly for each alloy sample. The Sb profile tails
of within ~1 μm which is more than the estimated distance for the film-substrate
transition region. However, there are several reasons why this tail-off region
should not be interpreted too closely at present. It probably reflects simul-
taneous sputtering of the film and substrate. This would be caused by a varia-
tion in the film thickness over the sample area. Also some slight rounding of
the sample occurs at the edges during sputtering. Finally, the difference in
the sputtering yields between the film and the substrate tends to exagerate the
depth of the transition region. In subsequent experiments it is suggested
that either a guard ring or a SiO_2 window be employed to minimize sample
rounding.

C. Electron Microprobe Investigations

In addition to using the electron microprobe to measure inhomogeneities
in crystals, we are also investigating the interaction of an electron beam
with III-V semiconductors. Thus, for example, we have used a clean vacuum
electron beam column to investigate cathodoluminescence of GaAs, GaP, and
$GaAs_xP_{1-x}$ semiconductors.[34] With this instrument (Figure 22), it is possible
to study the temperature dependence of cathodoluminescence down to 27°K with-
out contamination of the sample during electron irradiation. The system uses
a single liquid nitrogen cooled electron lens which also aids in reducing
sample contamination.[35] Irradiation times up to three hours with currents of
0.5 μA have resulted in no visible contamination on the semiconductor sample.
Accelerating voltages up to 50 kV and beam currents up to 1.5 μA with a spot
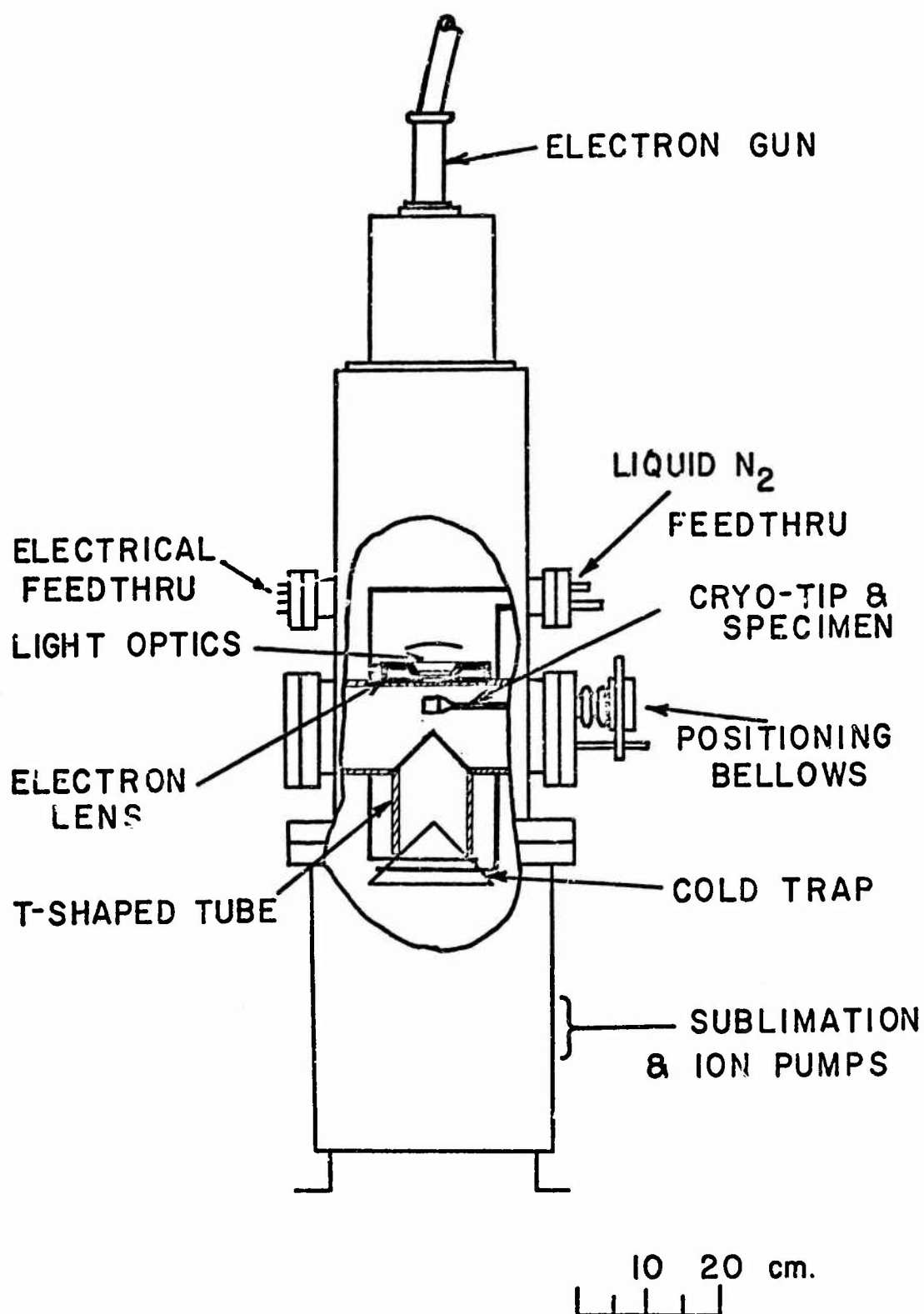size of 10-15 μm are obtained.

Figure 22. Schematic diagram of the electron beam column with approximate scale.

Figure 23 shows the peak of the cathodoluminescence spectrum of a heavily doped p-type GaAs sample irradiated with 50 kV electrons as a function of temperature. The dashed curve is a plot of the absorption edge of GaAs versus temperature according to Casey and Panish.[36] Experiments were performed on lightly doped p-type GaAs ($N_A = 7 \times 10^{16}$ cm^{-3}). The cathodoluminescence spectrum taken at 80°K and 50 kV is shown in Figure 24. Two emission peaks separated by 11 meV are seen. Cusano attributes the 1.487 eV peak to conduction band-isolated acceptors recombination.[37] The 1.499 eV peak is probably due to conduction band-valence band recombination. At room temperature only one broad emission band is observed.

Figure 25 shows a cathodoluminescence spectrum of GaP taken at 27°K with an accelerating voltage of 50 kV, a beam current of 5 nA and a spot size of 10 μm. It was expected that donor-acceptor pair recombination as reported by Thomas, et. al.,[38] at 1.6°K could be observed between 2.2 eV and 2.3 eV. However, donor-acceptor pair recombination showing spectra of resolved peaks in GaP has not yet been reported above 20°K. Shown in Figure 25 is the 'A' line due to the nitrogen bound exciton and the C bound-exciton line due to neutral sulfur donors.[39] The F line is due to recombination at pairs of isoelectronic nitrogen traps.[39] The other peaks could be phonon-replicas of the A line as discussed by Dean and Thomas.[40]

Future work will consist of the analysis of cathodoluminescence of $GaAs_xP_{1-x}$ mixed crystals as a function of temperature, current, and possibly voltage to determine the nature of the various recombination mechanisms in these crystals.

Stimulated emission is also being studied. When a semiconductor is bombarded with a focused electron beam it is possible for the region excited to have dimensions of the same order as the wavelength of the radiation due to recombination of excess hole-electron pairs. Under these conditions, many of the excess hole-electron pairs are in the near field of the radiation pattern produced by recombination of some of the excess hole-electron pairs. Thus, even in the absence of feedback from a cavity, it should be possible to observe stimulated emission if the electron probe has sufficiently high current density. In order to observe this phenomenon, an apparatus has been constructed which can be used to study electron beam excited luminescence at room temperature or liquid nitrogen temperature either with or without a magnetic field. Cathodo-
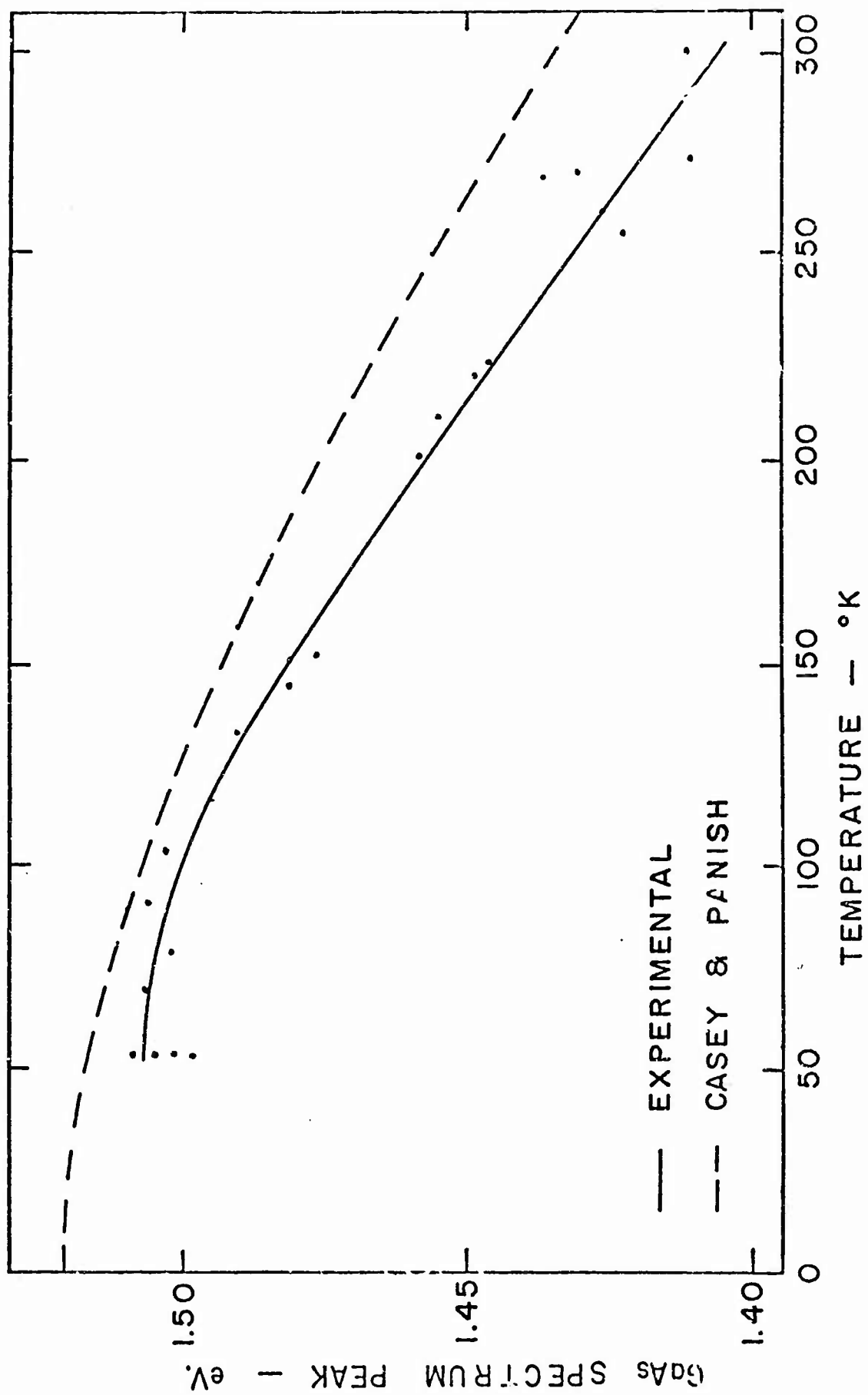
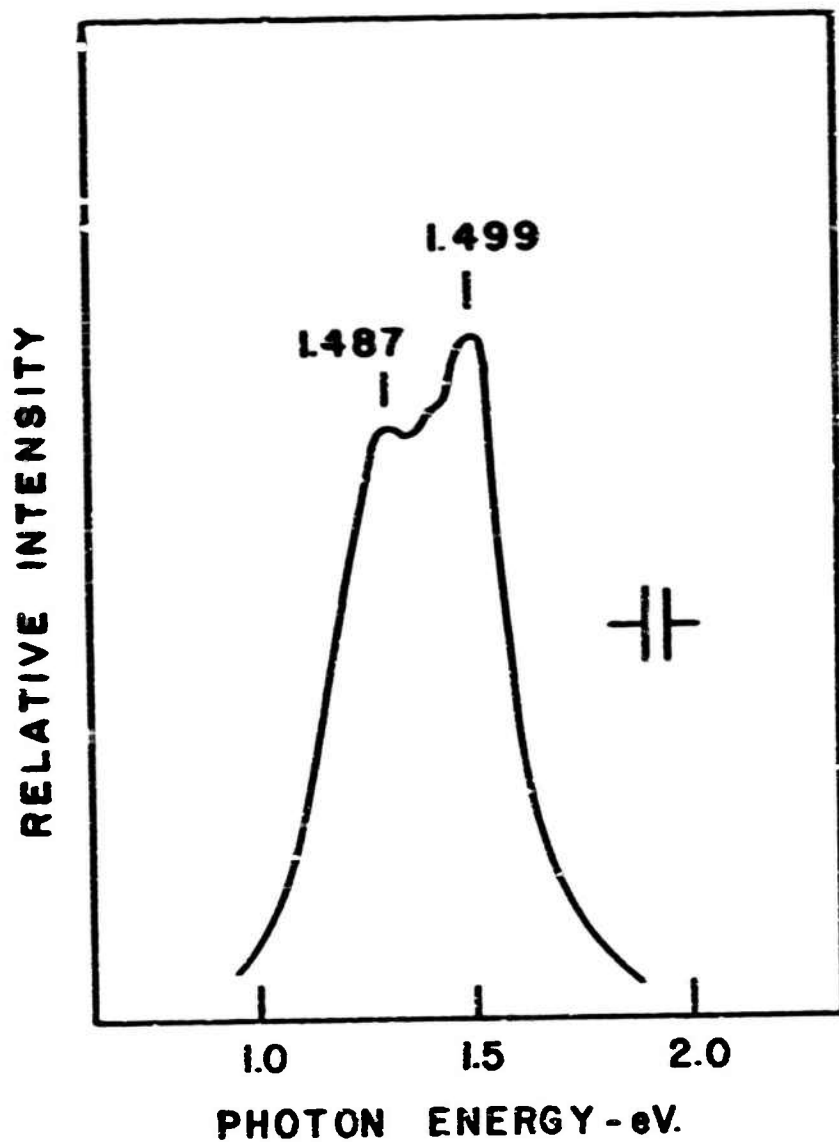Figure 23. Peak of the cathodoluminescence spectrum versus temperature of a heavily doped p-type GaAs sample.

Figure 24. Cathodoluminescence spectrum of p-type GaAs $N_A = 7 \times 10^{16}$ cm^{-3} at approximately 80°K.
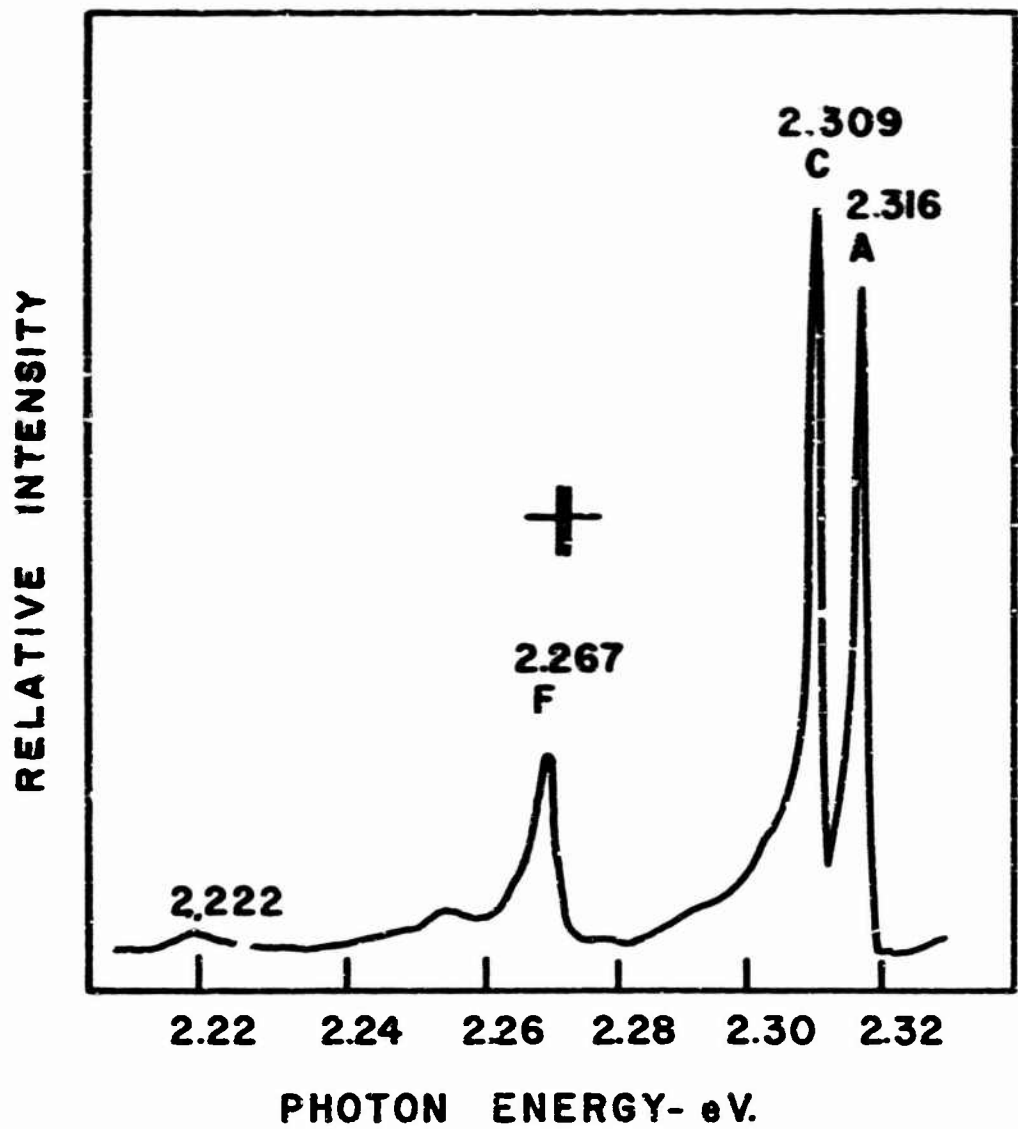
Figure 25.   Cathodoluminescence spectrum of GaP at 27°K.

luminescence on several heavily doped n-type GaAs samples has been investigated
using an electron probe X-ray microanalyzer (EMX-SM). So far we have not been
able to duplicate the results obtained at room temperatures by Casey and
Kaiser[41] and attributed by them to stimulated emission. Further experiments
are being made at low temperature and also at room temperature using more
carefully selected focusing conditions for the electron probe to optimize the
current density.

Crystallographic effects are observed in scanning electron beam instruments
because the angle of incidence of the electron beam on the specimen changes. In
most cases, the results obtained are a mixture of "topographic contrast" and
"crystallographic contrast" because both the position and angle of the electron
beam changes during the scan.

For the study of semiconductor materials, particularly III-V semiconductors
and their alloys, it would be useful to have a scanning system in which the beam
position remains fixed and the angle of incidence is scanned or the electron beam
position is scanned and the angle of incidence remains fixed. The former possi-
bility has been previously described.[42-44] The latter possibility has not
previously been used, but appears to have great potential for studies of poly-
crystalline materials and for studies of local variations in the perfection of
single crystals due to deformation, to ion implantation, to the diffusion of
impurities or to the precipitation of impurities.

We have investigated scanning systems that would provide controlled
"crystallographic contrast" in scanning electron microscopy. Several types of
scanning systems have been conceived and one of these has been tested using an
electron probe microanalyzed (ARL EMX-SM) with an additional set of deflection
coils. Preliminary results using a test specimen consisting of a bicrystal of
silicon are shown in Figure 26. Detailed description of the scanning methods
is given in Ref. 45. The techniques described in this paper should be of
great value in the study of III-V semiconductor materials.

D. Hall Effect Apparatus

A flexible Hall effect system has been designed to provide improved
diagnostic measurements. The system will use a variable temperature top loading
dewar system for the temperature range 4°K to 300°K and will feature a high
sensitivity, high impedance ($\sim 10^{12}$ Ω) differential amplifier with capacitive

Figure 26. Area and angle scans obtained on a silicon bicrystal: (a) an angle scan of the (111) oriented crystal (area 1); (b) an angle scan of the twin (area 2); (c) an area scan with beam angle A; and (d) an area scan with beam angle B. The scale of the area scan is indicated by the marker which is 100 microns long.

29-A

degeneration in the input circuitry. The components for this system and the dewar have been received. The magnetic field system has been calibrated and the temperature calibration of the dewar system is in progress. A circuit for low impedance Hall measurements is operational and the high impedance circuitry is near completion.

E. Tunnel and Thermal Effects in Photoemission from Schottky Barriers

Photoexcitation of carriers from a metal into a Schottky barrier depletion region has been recognized as providing the most direct and unequivocal measure of the barrier height. As such, it affords a prime diagnostic tool for analysis of impurity and interface effects in experimental semiconductor materials. Because of this we have been investigating two sources of error in interpreting these measurements.[46] In principle, such data should be analyzed by use of a Fowler plot.[47] It has been more customary, however, to choose an easier approximate curve fitting technique. A plot of $R^{1/2}$ (photoresponse per absorbed photon)$^{1/2}$ versus photon energy, becomes nearly linear when $h\nu - \phi_B \gg kT$ (cf., Figure 27). The intercept of the asymptotic curve occurs when $h\nu = \phi_B$ within the framework of the Fowler model. In Figure 28 we show a simple universal curve which can be used to correct the approximate curve fitting procedure. This procedure in effect allows for photoexcitation of electrons in the Fermi tail of the electron distribution in the metal and eliminates the cut and try associated with the Fowler curve fitting procedure.

The above approach is also a useful way to express the corrections associated with photon assisted tunneling through or over a Schottky barrier. We have evaluated these corrections by appropriately weighting the photoexcited electron distribution with transmission coefficients obtained by a computer analysis using techniques similar to those of Crowell and Sze.[48] The model used for the transmission coefficient incorporates image force effects, Thomas-Fermi field penetration into the metal, effective mass differences in the metal and semiconductor conservation of transverse crystal momentum and effects of total band bending in the semiconductor. Results for selected doping and band bending for metal n-type GaAs systems are shown in Figure 29. Due to the small effective mass of electrons in GaAs, these corrections become appreciable for doping $\sim 10^{18}$ cm^{-3}. These data provide the corrections to the image force
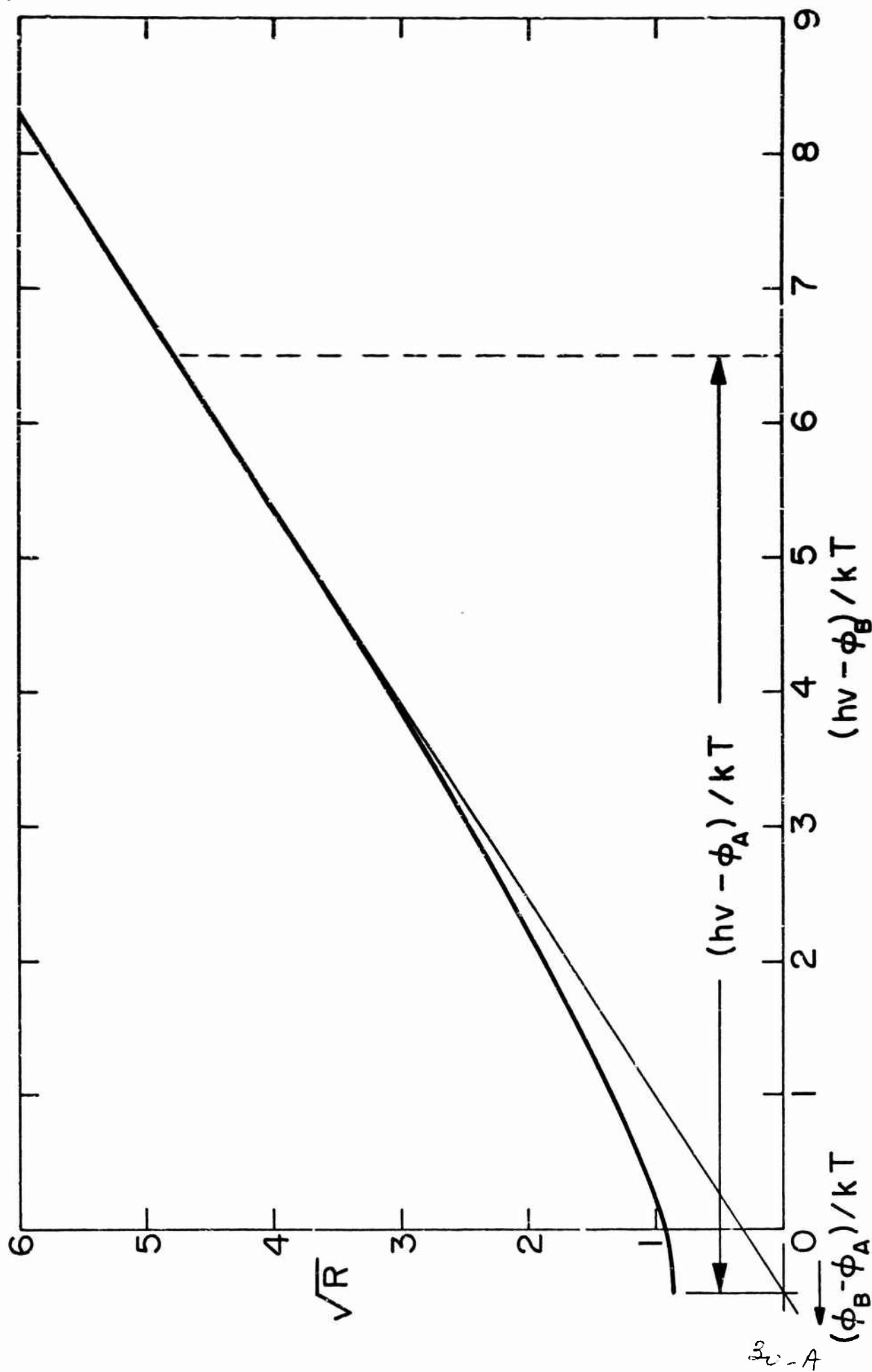
Figure 27. (Photoresponse per absorbed photon)$^{1/2}$ versus (photon energy-barrier height) in units of kT according to the Fowler[47] theory, and construction to find the apparent barrier height at given photon energy.
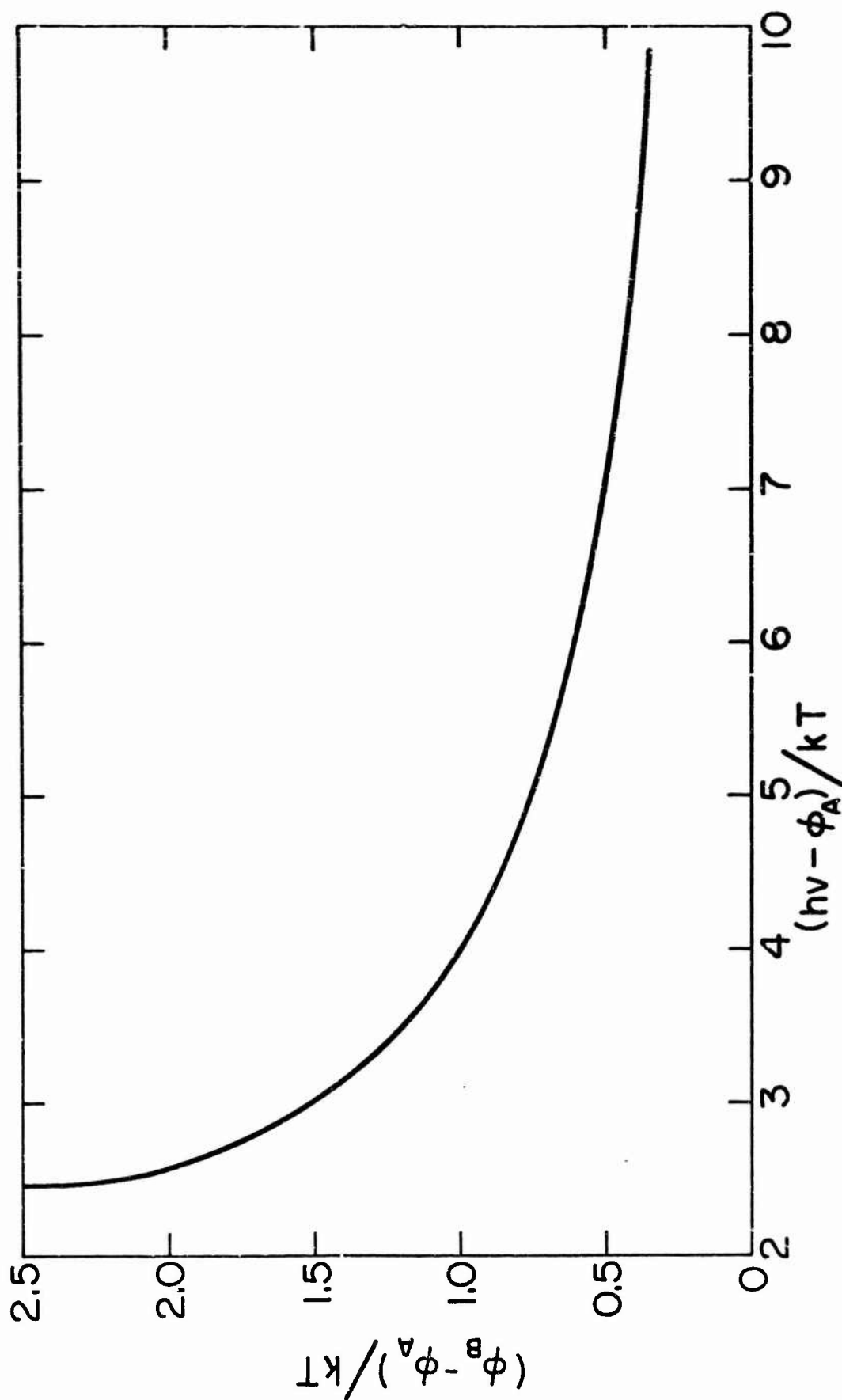
Figure 28. Relationship between apparent and true barrier height versus $(h\nu - q\phi_A)$ all in units of kT.
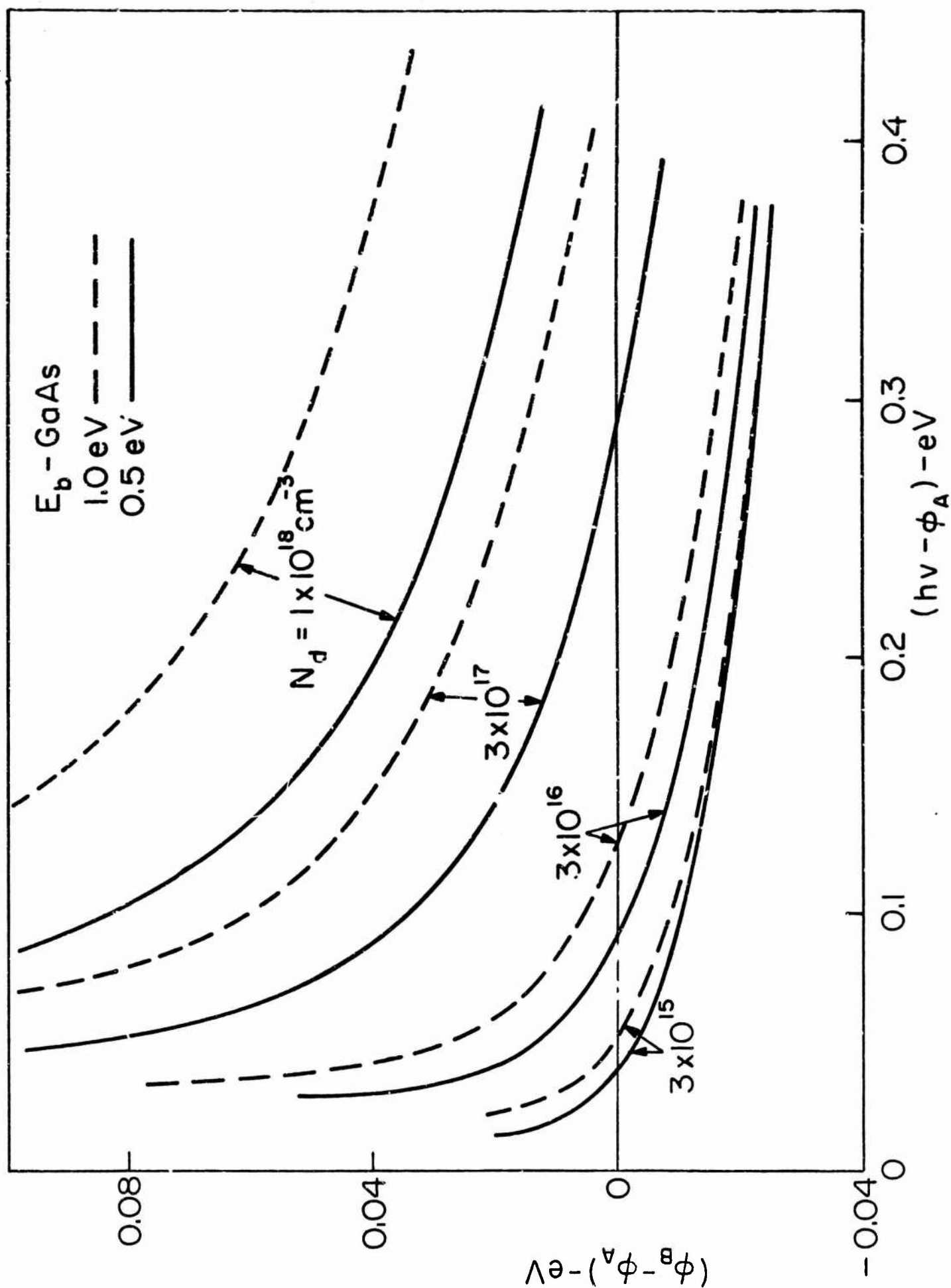
3υ -B

Figure 29. Correction to apparent barrier height due to tunneling for a free electron metal - n-type GaAs system.

lowered barriers. The corresponding results for Si show smaller contributions due to tunneling, but an appreciable effect due to conservation of transverse momentum. This work will be submitted for publication on completion of the calculations for Si.

F. Capacitance Effects of Deep Level Impurities in Schottky Barriers

Deep-level impurities in semiconductors have many undesirable effects and are most frequently found in new semiconducting materials and in lightly doped materials. The nature of their intrinsic behavior has not in general been well defined, especially in the area of capacitance effects. We seek to clarify this problem so that the interference of deep-level impurities on capacitance impurity profiles can be more clearly diagnosed and the energy levels and capture cross sections of the deep levels themselves can be determined comparatively in Schottky barrier systems. We plan to use guide-lines established by a program of investigation on Si Schottky barriers (funded by the Army Research Office, Durham) in investigations of III-V semiconductors. The following theoretical results were obtained using Joint Services Electronics Program and ARPA support during the initial stages.[49]

A typical Schottky barrier energy band diagram is shown in Figure 30 where one deep donor and one shallow donor level are present. The deep level is ionized mainly when above the bulk Fermi line. The charge density increment for an incremental change in surface potential is also shown. At zero frequency, the center of charge (or effective capacitance spacing) is shown schematically by x_{dc}. At a frequency ω, however, the dotted portion of this distribution does not respond and the effective capacitance spacing becomes x_ω. At high enough frequencies that the deep level cannot respond, the spacing becomes $x_{\omega h}$ which is determined by the free electron density in the conduction band. If we assume the validity of Shockley-Read recombination statistics,

$$\omega = \omega(\psi) = \sigma v(n(\psi) + n_1(\psi_i))$$

where σ is the capture cross section for electrons, v is the electron thermal velocity and $n(\psi)$ the electron density where the electron potential energy is a relative to the bulk Fermi energy ($\omega_1 \equiv \sigma v n_1(\psi_i)$). If we assume that at
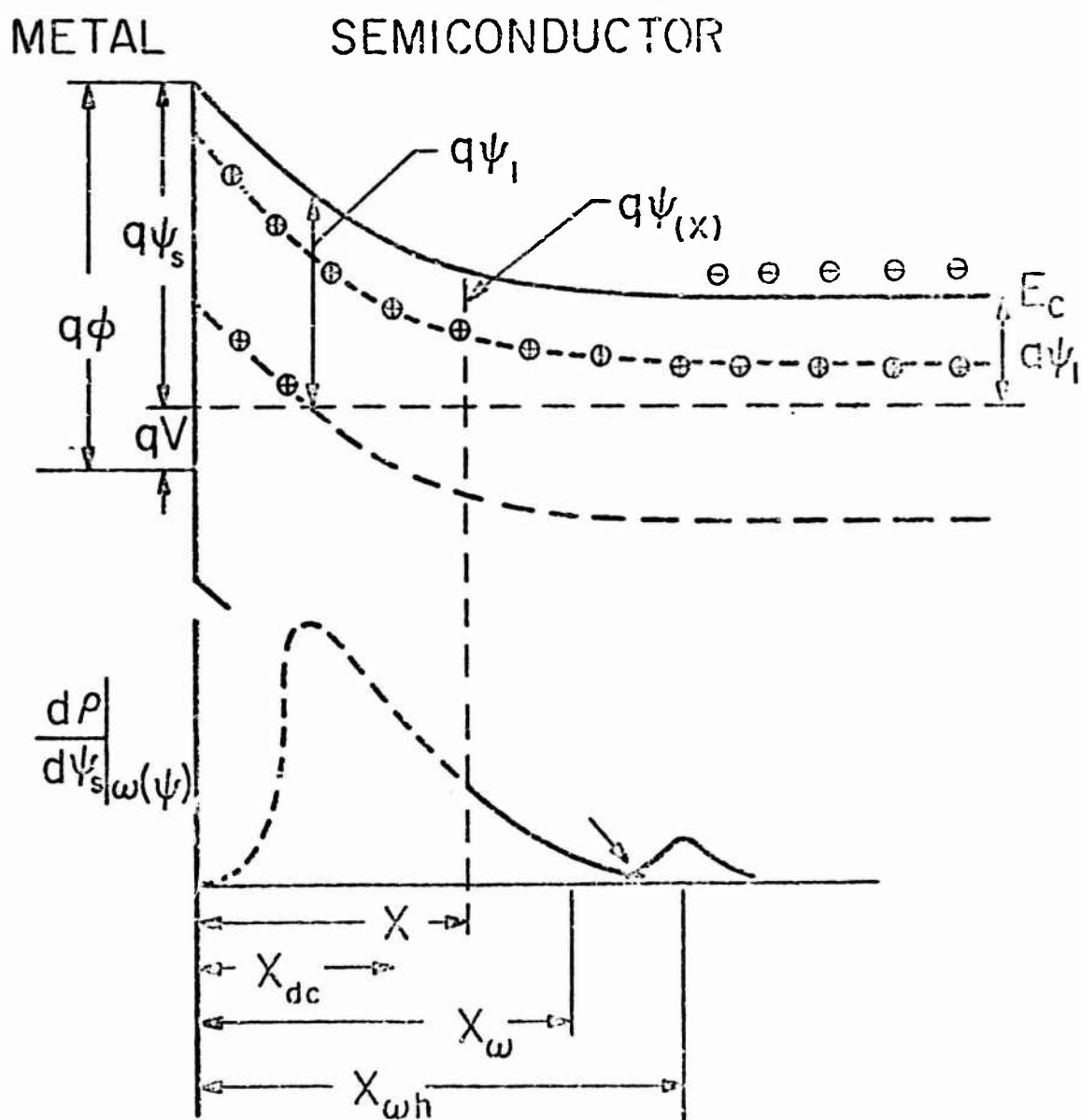
Figure 30. Electron energy band diagram for Schottky barrier with deep and shallow level impurities plus schematic illustration of geometrical distribution of charge increments for d-c voltage increments (solid plus dashed line) and a voltage increment at frequency $\omega(\psi)$.

31-A

$u(\psi)$ only charges beyond x respond, then the frequency dependence of the capacitance $C(u,\psi_s)$ can be expressed in terms of the low frequency (d.c.) variable as follows:

$$\frac{1}{c(u,\psi_s)} - \frac{1}{c(0,\psi_s)} = \int_{u_s}^{u} \frac{1}{c(0,\psi)} \frac{d \ln}{d\psi} \frac{d\psi}{du} du \;.$$

Figure 31 shows the theoretical results in a form which applies for any bias such that $\psi_s \gg \psi_i$. The parameter C_D ($= [cq^2(N_D + N_s)/kT]^{1/2}$) can be obtained from the slope of $1/C^2$ versus V and the other three parameters which define the system are degree of freeze-out of the deep level ($c(\psi_i - \psi_F)/kT$), ratio of deep to shallow impurity concentrations, N_s/N_{d} for donors or $((N_s/N_{d}) - 1)$ for acceptors, and ω_1 the lowest frequency at which all deep level impurities respond. The dotted line shows an asymptotic result due to Schible and Milnes[50] which differs by a factor of four in elastance difference or a factor of 16 in capture cross section. The effects of freeze-out and ratio of shallow to deep impurity concentrations are far from orthogonal. Accordingly to assist in diagnosis, the frequency at which 90% of the transition has occurred, ω_9, has been chosen as additional parameter. Figure 32 shows the relationships between $C_D/C(0,\psi_s) - C_D/C(0,\psi_c)$ and ω_9/ω_1 as a function of N_s/N_D. Note that for a given elastance difference the frequency range defines a unique value of N_s/N_D and degree of freeze-out as long as N_s/N_D is not in the region of unity.

The above results show for the first time a method of deducing capture cross section, impurity energy level and ratio of shallow to deep level impurity from the capacitance-voltage relationship at a single temperature.

G. Experimental Techniques for Schottky-Barrier Capacitance-Voltage Studies

Development of an active capacitance probe front-end for a direct reading capacitance-voltage diagnostic system has been completed. Analysis of the behavior of active probe designs revealed a trade-off between minimum frequency of measurement and leakage current of the device under test. Experiments verified the existence of this trade-off. Several modifications of the unit were developed and a final design settled upon. The completed unit can measure
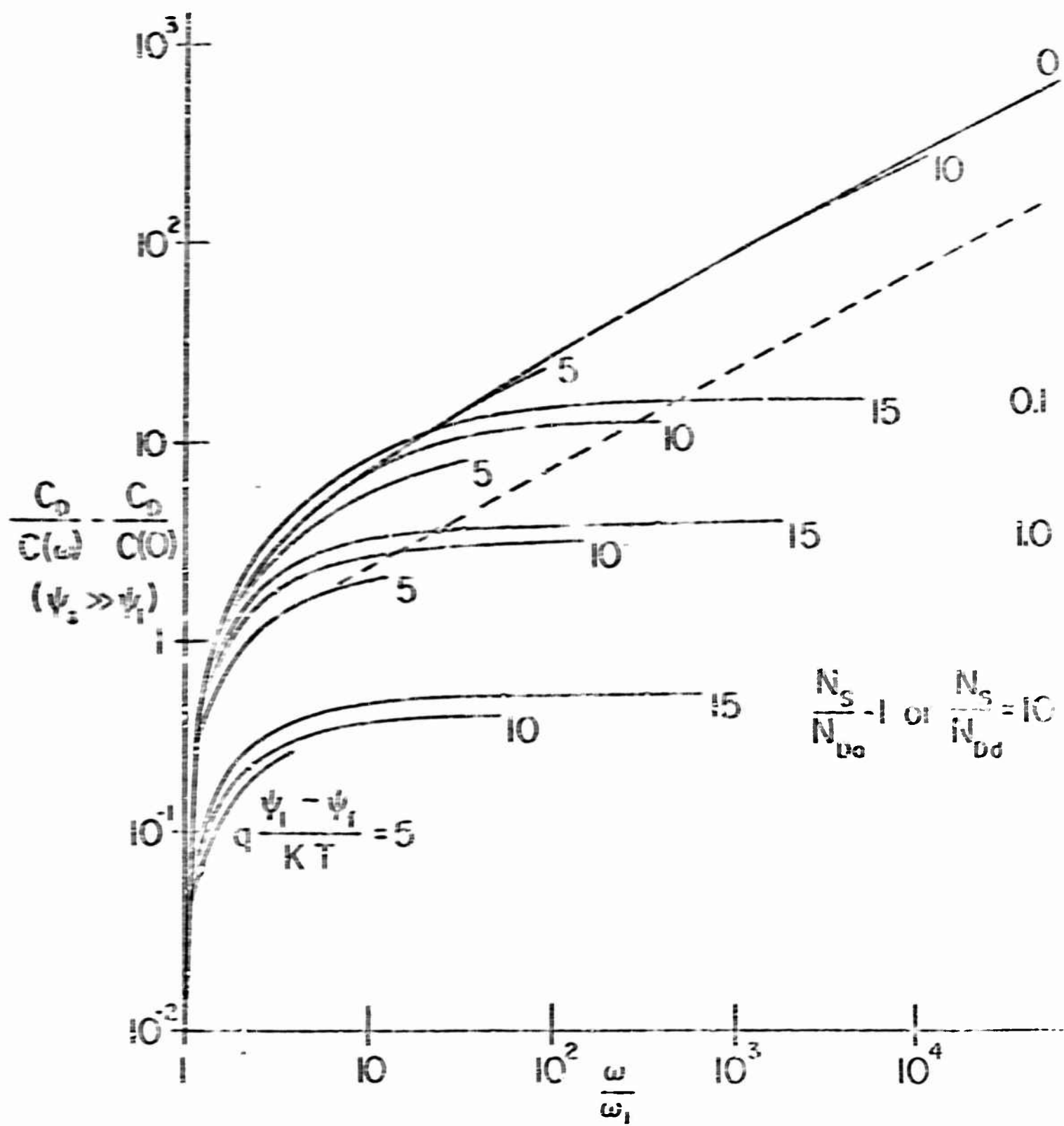
Figure 31. Normalized elastance difference between frequencies ω_1 and ω versus ω in units of ω_1 for selected degrees of freezeout $\left(\dfrac{q(\psi_1-\psi_i)}{kT}\right)$ and ratio of shallow to deep impurity concentrations. The dotted line gives the asymptotic results of Schibli and Milnes (12) for the case of $N_s = 0$.
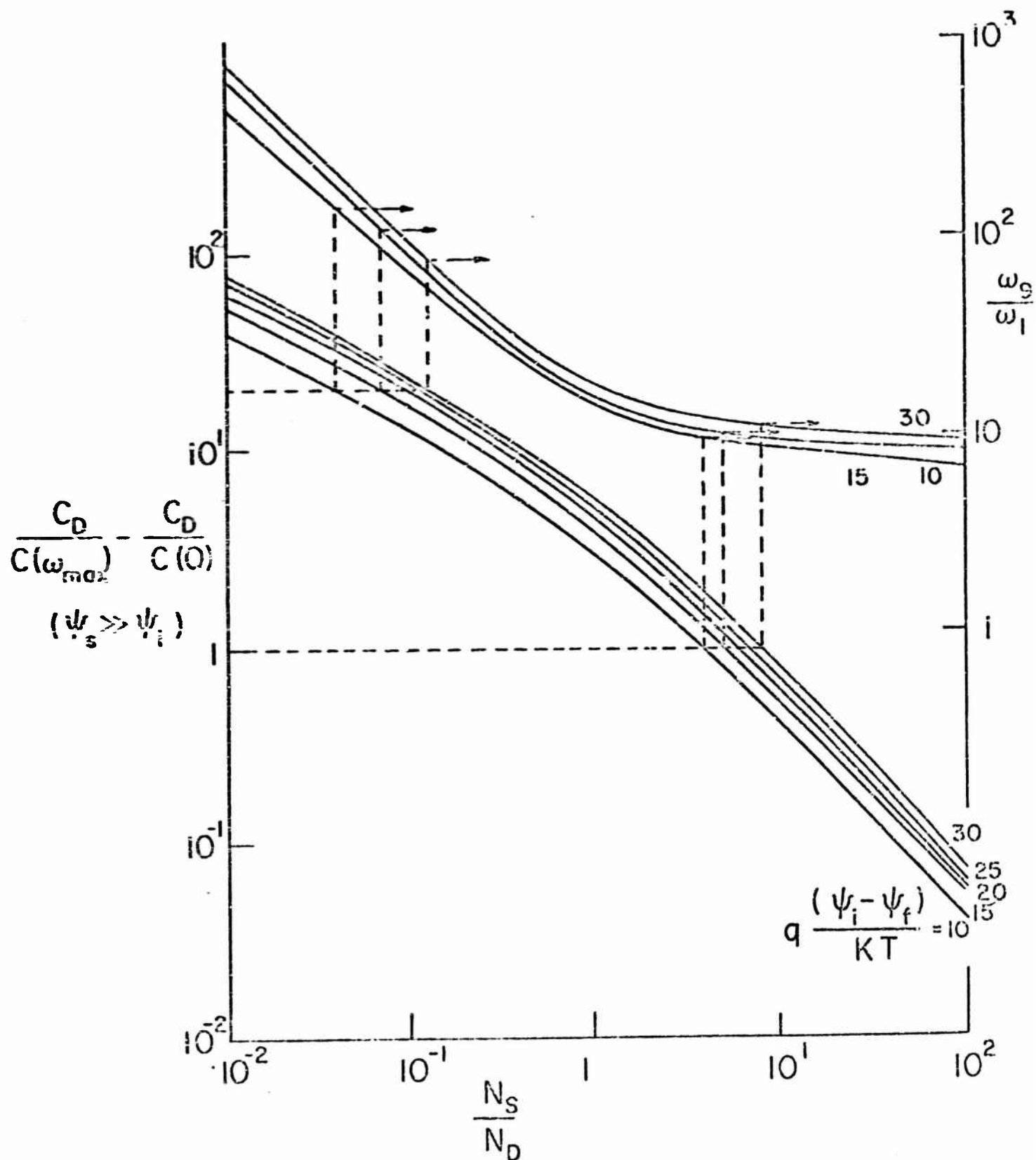
32-A

Figure 32.Maximum elastance (1/C) change and frequency interval for 90% of of the maximum elastance change as a function of N_s/N_{d_d} for selected degrees of impurity freezeout. Note the reversal of effects of freeze-out when $N_s/N_{d_d} < 1$ or > 1 for a given elastance change. 32-B

capacitance with less than one percent error at frequencies below 10 Hz up to 200 KHz and with leakage currents as high as 100 μA. The probe has sufficient electronic degeneration of capacitance to ground that remote operation with effective strays below 1 pF is possible.

Testing is underway on the two remaining units in the system: (1) a universal constant-voltage signal source unit, and (2) a general purpose logarithmic-algorithm analog computer unit. The signal source provides constant voltage sine-wave signals at two frequencies in the range 2 - 200 KHz, individually variable, with provision for amplitude and frequency modulation and sweep frequency generation. The unit also provides automatic D-C bias sweeping.
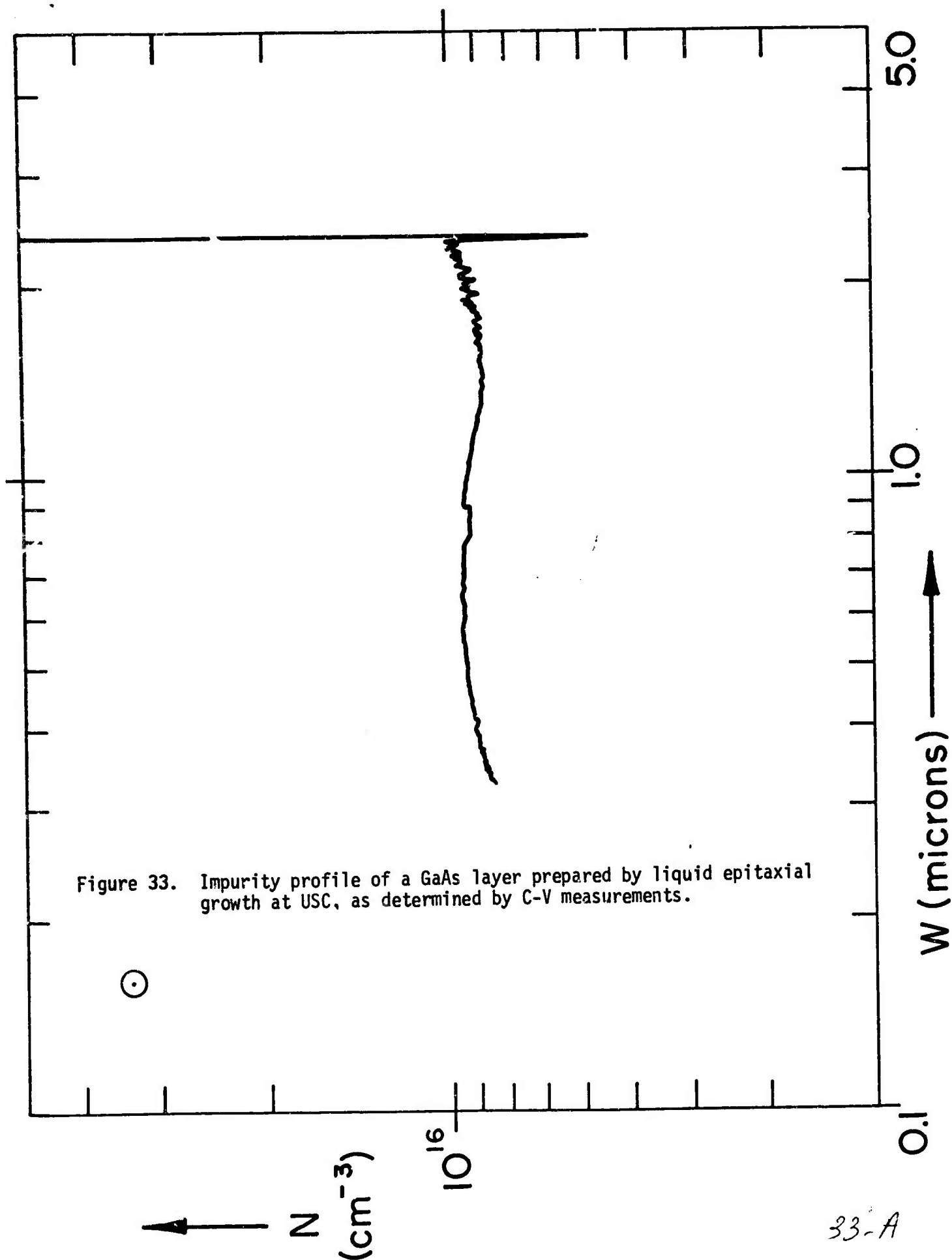
The general purpose computer unit allows extreme flexibility of output format for capacitance-voltage (C-V) and will be set up to display on-line analysis of capacitance-frequency (C-ω) measurements. It presently provides data for impurity profile determination in semiconductors. Additional programming is being developed to allow presentation of C-V and C-ω data in formats previously requiring extensive calculation.

The active probe unit output signals are analyzed by two lock-in amplifiers in series. Phase-sensitive amplification of the signals is provided at each step. This greatly reduces the effect of noise and sample leakage on the measurements. This feature is not easily available with bridge-type measurements. The output from the lock-in amplifiers is analyzed by the analog computer unit and the output plotted directly on an X-Y plotted. This system is currently undergoing testing and calibration.

A Schottky barrier C-V automatic "impurity profiler" has also been designed and built.[51] Carrier density versus distance is displayed as shown in Figures 33 and 34.

H. Photoluminescence Measurements

Photoluminescence spectra of liquid epitaxial grown films of $Ga_{1-x}In_xAs$ and $GaAs_{1-x}Sb_x$ alloys were measured at room temperature and at the boiling points of helium and nitrogen. In general, the evidence was that impurity-band transitions were most likely for the detected luminescence. For both alloy systems the same dependence of the energy gap on x was observed as the values of $x \rightarrow 0$ (within estimated errors < 0.02 eV). Photoluminescent efficiencies of

Figure 33. Impurity profile of a GaAs layer prepared by liquid epitaxial growth at USC, as determined by C-V measurements.
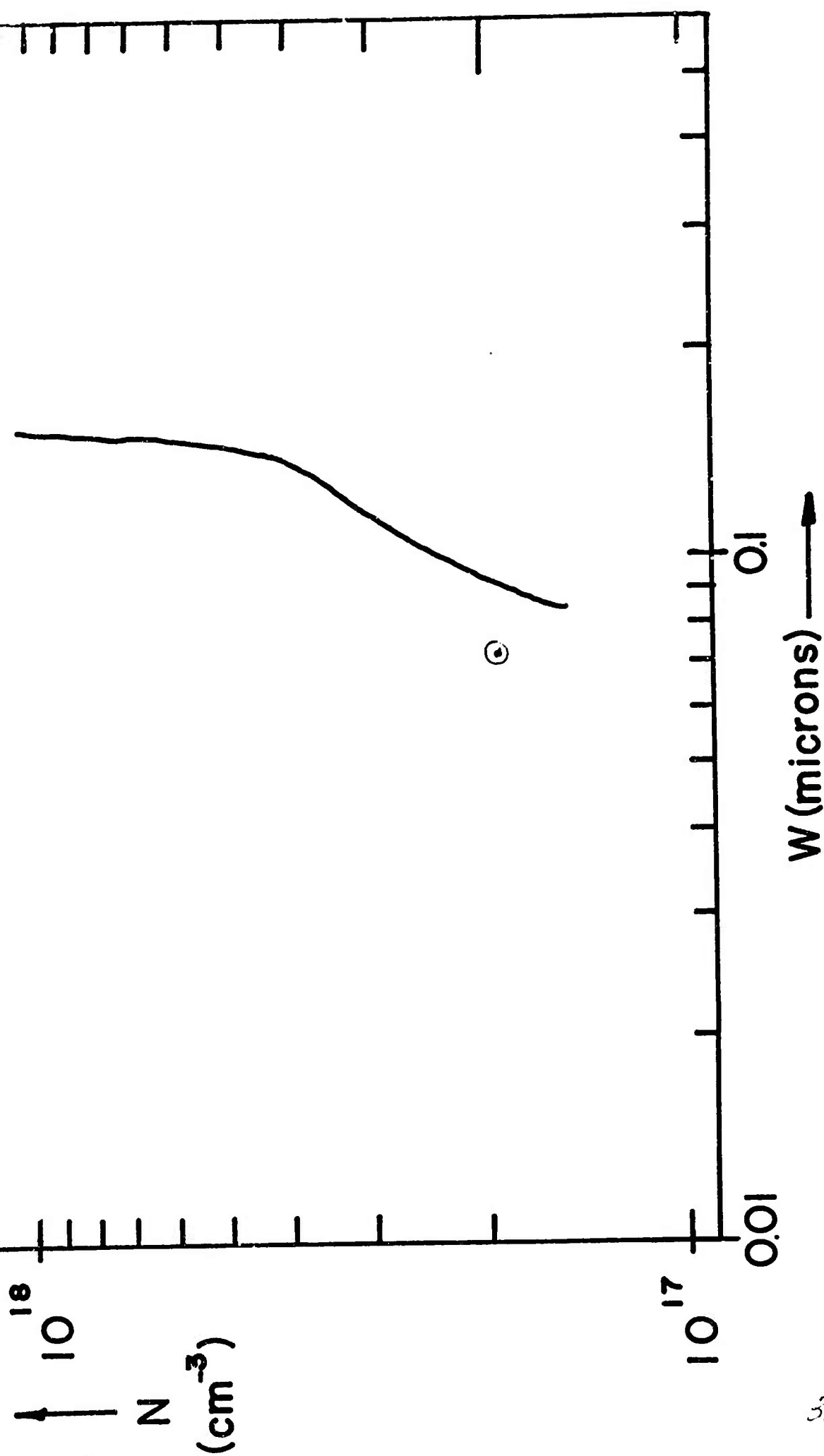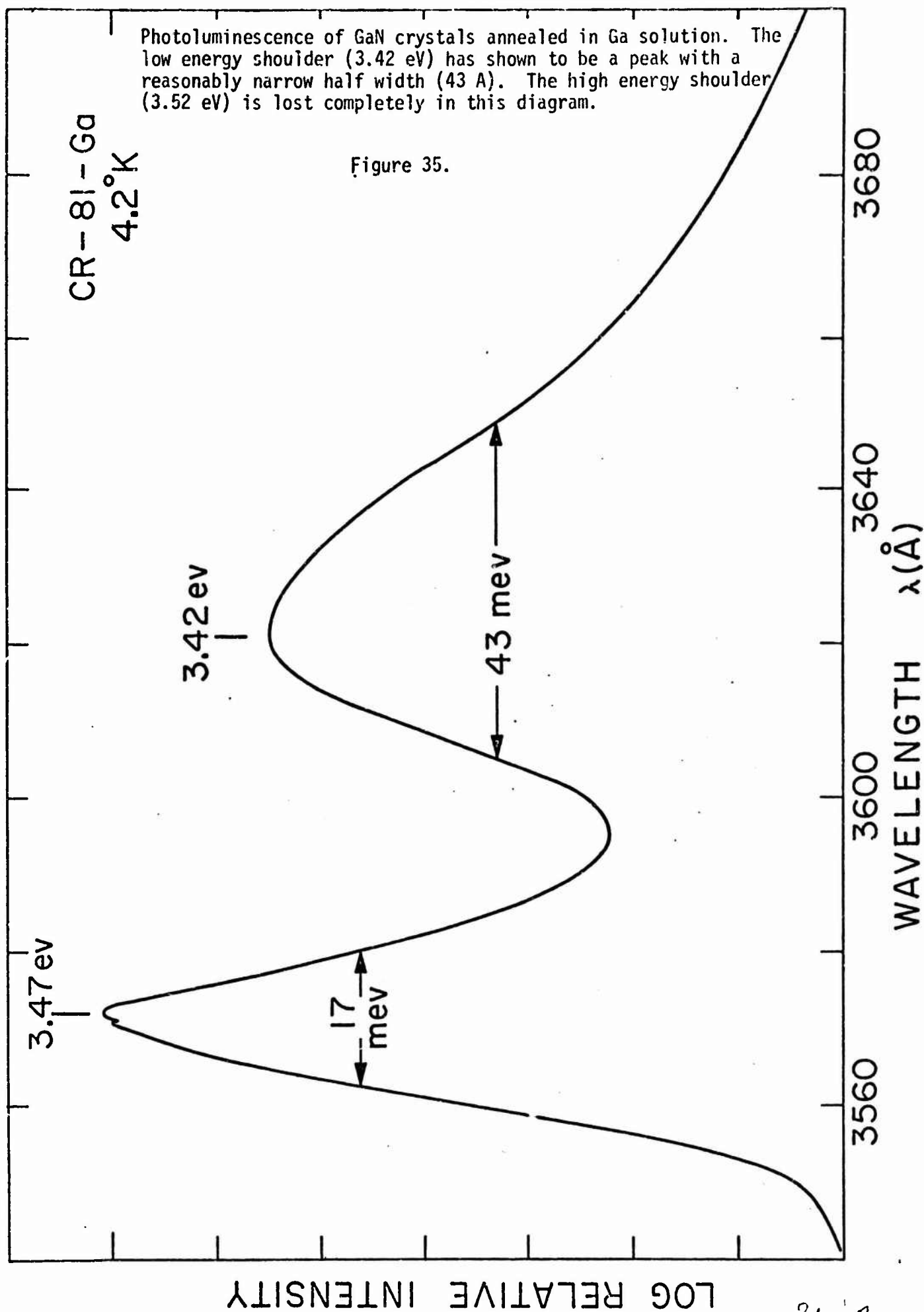
33-A

Figure 34. Impurity profile of hyperthin chemically vapor deposited epitaxial film of GaAs from the Monsanto Company as determined by C-V measurements.

33-B

the alloys were encouragingly good, i.e., within a factor of ten of solution-grown GaAs for values of $x \leq 0.06$. Relative widths of the spectral and X-ray diffraction peaks were consistent with alloy homogeneities, $\Delta x/x$, of 0.1 or better.

Highly efficient photoluminescence has been observed in GaN films at low temperatures and at room temperature. There are two peaks seen on all the samples measured: one at 3.47 eV which does not change with sample, and one at 3.42 or 3.448 eV depending on the sample used, as shown in Figures 35 and 36. The 3.47 eV peak is explained as due to free exciton transitions and the 3.42 eV (or 3.448 eV) may be due to bound exciton transitions. Li doped GaN has given a broad spectrum with high quantum efficiency. The spectrum covers a range from 3.57 to 3.16 eV.

Attempts were made to observe stimulated emission at liquid nitrogen temperature with a GaN Fabry-Perot structure. No evidence of lasing action was found in this experiment.

Photoluminescence of GaN crystals annealed in Ga solution. The low energy shoulder (3.42 eV) has shown to be a peak with a reasonably narrow half width (43 A). The high energy shoulder (3.52 eV) is lost completely in this diagram.
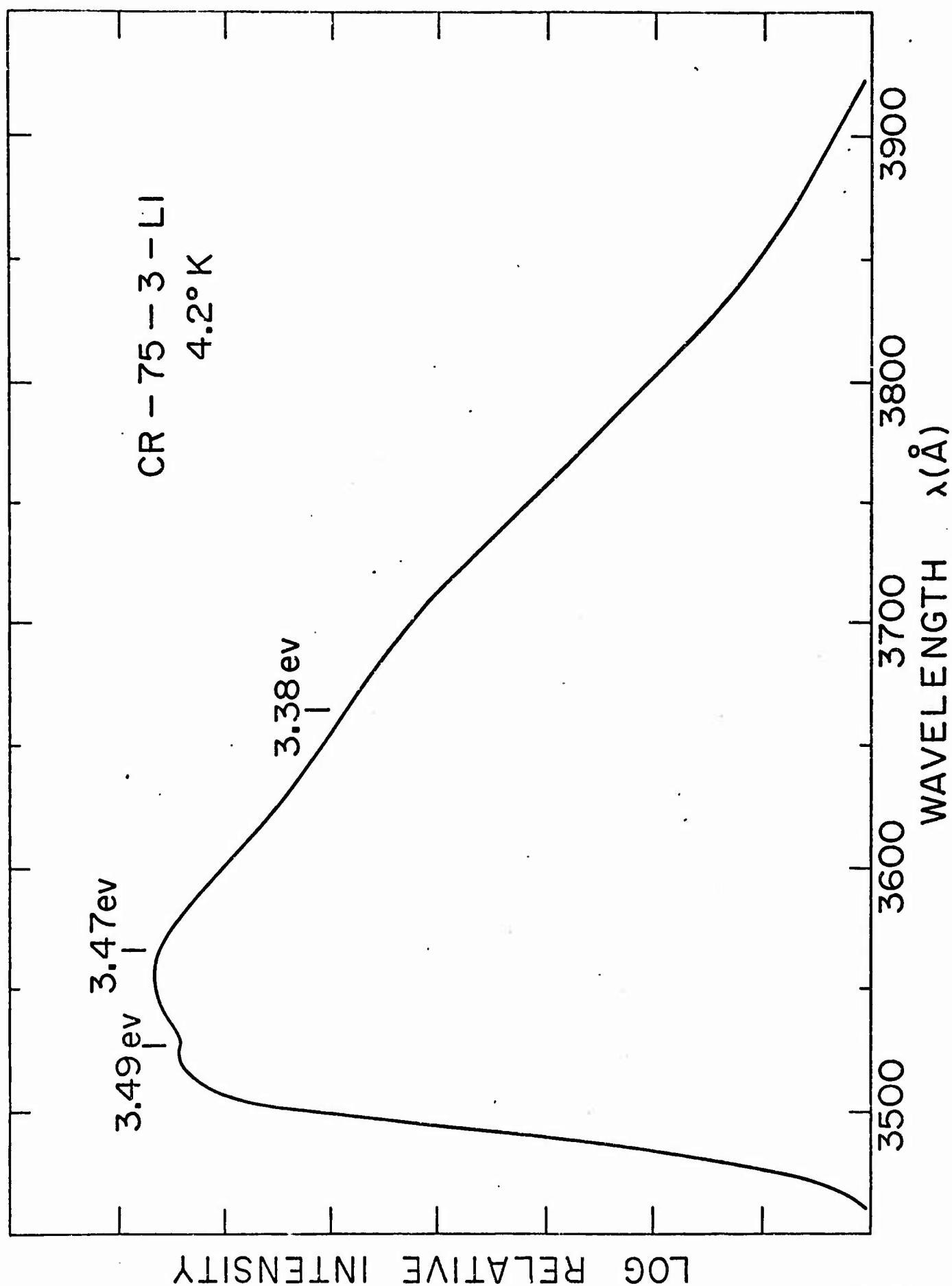
Figure 35.

Figure 36. Photoluminescence of GaN crystals grown over Ga boat. The low energy shoulder which appears at 3.448 eV in this case has higher luminescence efficiency then the 3.47 eV peak.

34B

REFERENCES

1. V. W. Poch, Glastechnische Berichte 37, 533 (1964).

2. Kirk-Othmer, "Boron Compounds," in The Encyclopedia of Chemical Technology, 2nd ed., Vol. 3 (1963).

3. R. M. Adams, "Boron, Metallo-Boron Compounds and Boranes," (1964).

4. H. Franz, Glastech. Ber. 38, 54 (1965).

5. *V. Yip and W. R. Wilcox, Bull. Am. Phys. Soc. 15, 1624 (1970).

6. *R. J. Baughman, R. A. Lefever and W. R. Wilcox, J. Crystal Growth 8, 317 (1971).

7. *W. R. Wilcox and A. Leon, J. Crystal Growth 8, 230 (1971).

8. W. R. Wilcox and P. J. Shlichta, J. Appl. Phys. 42, 1823 (1971).

9. T. R. Anthony and H. E. Cline, Phil. Mag. (in press).

10. *W. R. Wilcox, J. Crystal Growth (in press). Presented at International Conference on Crystal Growth 3, Marseille, France, 1971.

11. *W. R. Wilcox in Preparation and Properties of Solid State Materials, R. Lefever, ed. (Dekker, N. Y., 1971).

12. R. J. Walsh and A. H. Herzog, U.S. Pat. 3,170,273 (Feb. 23, 1965).

13. M. V. Sullivan and G. A. Kolb, J. Electrochem. Soc. 110, 585 (1963).

14. A. Reisman and R. Rohr, J. Electrochem. Soc. 111, 1425 (1964).

15. *J. E. Greene and J. M. Whelan (submitted for publication), Bull. Am. Phys. Soc. 15, 1614 (1970).

16. A. U. MacRae and G. W. Gobeli, J. Appl. Phys. 35, 1629 (1964).

17. P. L. Petrusevich and E. S. Sollertinskaya, Sov. Phys. Crystallography 8, 182-185 (1963).

18. E. P. Warekois and P. H. Metzger, J. Appl. Phys. 30, 960-962 (1959).

19. E. D. Jungbluth, J. Electrochem. Soc. 122, 580 (1965).

20. M. Yaskorokhod, L. Datsenko and A. Tkalenko, Sov. Phys. - Solid State 8, 593 (1966).

21. *J. E. Greene and J. M. Whelan (submitted for publication).

22. R. V. Stuart and G. K. Wehner, J. Appl. Phys. 35, 1819 (1964).

23. R. V. Stuart, K. Brower and W. Mayer, Rev. Sci. Instr. 35, 425 (1963).

24. J. Jeans, Kinetic Theory of Gases (University Press, Cambridge, 1967).

25. R. V. Stuart and G. K. Wehner, Phys. Rev. Letters 4, 409 (1960).

26. R. V. Stuart and G. K. Wehner, J. Appl. Phys. 33, 2345 (1962).

27. M. Kaminsky, Atomic and Ionic Impact Phenomena on Metal Surfaces (Academic Press, New York, 1965).

28. G. D. Magnuson and C. E. Carlston, J. Appl. Phys. 34, 3267 (1963).

29. A. L. Southern, W. R. Willis and M. T. Robinson, J. Appl. Phys. 34, 153 (1963).

30. M. T. Robinson and O. S. Oen, Appl. Phys. Letters 2, 30 (1963).

31. H. C. Gatos and M. C. Lavine, J. Electrochem. Soc. 107, 427 (1960).

32. National Bureau of Standards, Tables of Spectral Line Intensities, N.B.S. Monograph 32, Part 1.

33. C. T. Li, Ph.D. Dissertation, University of Southern California, 1971.

34. *H. C. Marciniak and D. B. Wittry, submitted to Rev. Sci. Instr.

35. H. Neuhaus, "Reduction of Contamination Effects in Electron Microprobe Analysis," Third National Conference on Electron Microprobe Analysis; Nov. 19, 1968.

36. M. B. Panish and H. C. Casey, Jr., J. Appl. Phys. 40, 163 (1969).

37. D. A. Cusano, Solid State Comm. 2, 353 (1964).

38. D. G. Thomas, J. J. Hopfield and K. Colbow, "Light from Distant Pairs," p. 67 in Radiative Recombination in Semiconductors (Paris, 1964).

39. M. Gershenzon, "Electroluminescence from p-n Junctions," p. 625-627, in Luminescence of Inorganic Solids (New York, 1966).

40. P. J. Dean and D. G. Thomas, Phys. Rev. 150, 690 (1966).

41. H. C. Casey, Jr., and R. H. Kaiser, Appl. Phys. Letters 8, 113 (1966).

42. D. B. Coates, Proc. 2nd Annual SEM Symposium, IITRI, Chicago, Illinois, (1969), p. 29-40.

43. C. G. VanEssen and E. M. Shulson, J. Mt. Sci. 4, 336 (1969).

44. C. G. VanEssen, E. M. Schulson and R. H. Donaghay, Nature 225, 847 (1970).

45. D. B. Wittry, submitted to Brit. J. Phys. D.

46. *C. R. Crowell, T. W. Kao and V. L. Rideout, Bull. Am. Phys. Soc. <u>15</u>, 1615 (1970).

47. R. H. Fowler, Phys. Rev. <u>38</u>, 45 (1931).

48. C. R. Crowell and S. M. Sze, J. Appl. Phys. <u>37</u>, 2683 (1966).

49. *K. Nakano and C. R. Crowell, Bull. Am. Phys. Soc. <u>15</u>, 1614 (1970).

50. E. Schibli and A. G. Milnes, Solid State Electron. <u>11</u>, 323 (1968).

51. B. J. Gordon, H. L. Stover and R. S. Hark in "Proceedings of the Symposium on Silicon Device Processing," American Society for Testing and Materials, 1970.

52. *Y. Okuto and C. R. Crowell, "High Field Impact Ionization in the Baraff Approximation," Bull. Am. Phys. Soc. <u>15</u>, 1615 (1970).